

USING THE TILTED FLAT- Λ CDM AND THE UNTILTED NON-FLAT Λ CDM INFLATION MODELS TO MEASURE COSMOLOGICAL PARAMETERS FROM A COMPILATION OF OBSERVATIONAL DATACHAN-GYUNG PARK¹ AND BHARAT RATRA²(Dated: July 29, 2019)
Draft version July 29, 2019

ABSTRACT

We use the physically-consistent tilted spatially-flat and untilted non-flat Λ CDM inflation models to constrain cosmological parameter values with the Planck 2015 cosmic microwave background (CMB) anisotropy data and recent Type Ia supernovae measurements, baryonic acoustic oscillations (BAO) data, growth rate observations, and Hubble parameter measurements. The most dramatic consequence of including the four non-CMB data sets is the significant strengthening of the evidence for non-flatness in the non-flat Λ CDM model, from 1.8σ for the CMB data alone to 5.1σ for the full data combination. The BAO data is the most powerful of the non-CMB data sets in more tightly constraining model parameter values and in favoring a spatially-closed Universe in which spatial curvature contributes about a percent to the current cosmological energy budget. The untilted non-flat Λ CDM model better fits the large-angle CMB temperature anisotropy angular spectrum and is more consistent with the Dark Energy Survey constraints on the current value of the rms amplitude of mass fluctuations (σ_8) as a function of the current value of the nonrelativistic matter density parameter (Ω_m) but does not provide as good a fit to the smaller-angle CMB temperature anisotropy data as does the tilted flat- Λ CDM model. Some measured cosmological parameter values differ significantly between the two models, including the reionization optical depth and the baryonic matter density parameter, both of whose 2σ ranges (in the two models) are disjoint or almost so.

Subject headings: cosmological parameters — cosmic background radiation — large-scale structure of universe — inflation — observations — methods:statistical

1. INTRODUCTION

In the standard spatially-flat Λ CDM cosmogony (Peebles 1984) the cosmological constant Λ dominates the current energy budget, cold dark matter (CDM) and baryonic matter are the second and third biggest contributors to the cosmological energy budget now, followed by small contributions from neutrinos and photons. For reviews of this model, see Ratra & Vogeley (2008), Martin (2012), and Huterer & Shafer (2017). Many different observations are largely consistent with the standard picture, including CMB anisotropies data (Planck Collaboration 2016), BAO distance measurements (Alam et al. 2017), Hubble parameter observations (Farooq et al. 2017), and Type Ia supernova (SNIa) apparent magnitude data (Betoule et al. 2014). However, there still is room for mild dark energy dynamics or a bit of spatial curvature, among other possibilities.

The standard model is characterized by six cosmological parameters that are conventionally taken to be: $\Omega_b h^2$ and $\Omega_c h^2$, the current values of the baryonic and cold dark matter density parameters multiplied by the square of the Hubble constant H_0 (in units of $100 \text{ km s}^{-1} \text{ Mpc}^{-1}$); θ_{MC} , the angular diameter distance as a multiple of the sound horizon at recombination; τ , the reionization optical depth; and A_s and n_s , the amplitude and spectral index of the (assumed) power-law primordial scalar energy density inhomogeneity power spectrum (Planck Collaboration 2016). The standard model assumes a flat spatial geometry (Planck Collaboration 2016).

However, using a physically consistent non-flat inflation model power spectrum of energy density inhomogeneities

(Ratra & Peebles 1995; Ratra 2017), Ooba et al. (2018a) recently found that Planck 2015 CMB anisotropy measurements (Planck Collaboration 2016) do not require flat spatial geometry in the six parameter non-flat Λ CDM model. In the non-flat Λ CDM model, compared to the flat- Λ CDM model, there is no simple tilt option so n_s is no longer a free parameter and is replaced by the current value of the spatial curvature density parameter Ω_k .³

In non-flat models non-zero spatial curvature sets the second, new length scale. This is in addition to the Hubble length scale. Inflation provides the only known way to define a physically consistent non-flat model power spectrum. For open spatial geometry the open-bubble inflation model of Gott (1982) is used to compute the non-power-law power spectrum (Ratra & Peebles 1994, 1995).⁴ For closed spatial geometry Hawking's prescription for the quantum state of the universe (Hawking 1984; Ratra 1985) can be used to construct a closed inflation model that can be used to compute the non-power-law power spectrum of energy density inhomogeneities (Ratra

³ The CMB anisotropy data also do not require flat spatial geometry in the seven parameter non-flat XCDM inflation model (Ooba et al. 2018b; Park & Ratra 2019). Here the equation of state relating the pressure and energy density of the dark energy fluid is $p_X = w_0 \rho_X$ and w_0 is the additional, seventh, parameter. XCDM is often used to model dynamical dark energy but is not a physically consistent model as it cannot describe the evolution of energy density inhomogeneities. Also, XCDM does not accurately model ϕ CDM (Peebles & Ratra 1988; Ratra & Peebles 1988) dark energy dynamics (Podariu & Ratra 2001). In the simplest, physically consistent, seven parameter non-flat ϕ CDM inflation model (Pavlov et al. 2013) — in which a scalar field ϕ with potential energy density $V(\phi) \propto \phi^{-\alpha}$ is the dynamical dark energy and $\alpha > 0$ is the seventh parameter that governs dark energy evolution — Ooba et al. (2018c) again found that CMB anisotropy data do not require flat spatial hypersurfaces (also see Park & Ratra 2018a). (In both the non-flat XCDM and ϕ CDM cases, n_s is again replaced by Ω_k .)

⁴ For early discussions of observational consequences of the open inflation model, see Kamionkowski et al. (1994), Górski et al. (1995), and Górski et al. (1998).

¹ Division of Science Education and Institute of Fusion Science, Chonbuk National University, Jeonju 54896, South Korea; e-mail: park.chan.gyung@gmail.com

² Department of Physics, Kansas State University, 116 Cardwell Hall, Manhattan, KS 66506, USA; e-mail: ratra@phys.ksu.edu

2017). Both these open and closed inflation models are slow-roll inflation models (Gott 1982; Hawking 1984; Ratra 1985) so the resulting energy density inhomogeneity power spectra are untitled (Ratra & Peebles 1995; Ratra 2017).

Non-CMB observations, even combinations thereof to date, do not rule out non-flat dark energy models (see, e.g., Farooq et al. 2015; Cai et al. 2016; Chen et al. 2016; Yu & Wang 2016; L’Huillier & Shafieloo 2017; Farooq et al. 2017; Li et al. 2016; Wei & Wu 2017; Rana et al. 2017; Yu et al. 2018; Mitra et al. 2018, 2019; Ryan et al. 2018, 2019; Park & Ratra 2018b). The most restrictive constraints on spatial curvature come from CMB anisotropy measurements, but, as shown by Ooba et al. (2018a), when the correct non-power-law power spectrum for energy density inhomogeneities is used for the CMB anisotropy analyses, a spatial curvature density parameter contribution of magnitude a percent or two is still allowed, with the CMB anisotropy data (Planck Collaboration 2016) favoring a mildly closed model. Ooba et al. (2018a) also added a few BAO distance measurements to the mix and found that a mildly closed model was still favored. Moreover, the mildly closed model better fits the observed low- ℓ CMB temperature anisotropy multipole number (ℓ) power spectrum C_ℓ and was more consistent with rms fractional energy density inhomogeneity averaged over $8h^{-1}$ Mpc radius spheres, σ_8 , current values determined from weak lensing observations, although the flat- Λ CDM model better fits the observed higher- ℓ C_ℓ ’s.

In this paper we examine the constraints on the non-flat Λ CDM inflation model that result from a joint analysis of the Planck 2015 CMB anisotropy data (Planck Collaboration 2016), the Joint Light-curve Analysis (JLA) SNIa apparent magnitude measurements (Betoule et al. 2014), and all reliable BAO distance, growth factor, and Hubble parameter measurements to date. We also perform a similar analysis for the tilted flat- Λ CDM inflation model.

The main purposes of our analyses here are, firstly, to examine the effect that the inclusion of a significant amount of reliable, recent, non-CMB data has on the finding of Ooba et al. (2018a) that the Planck 2015 CMB anisotropy observations and a handful of BAO distance measurements are not inconsistent with the untitled closed- Λ CDM inflation model, and, secondly, to use this large new compilation of reliable non-CMB data to examine the consistency between the cosmological constraints of each type of data and to more tightly measure cosmological parameters than has been done to date.

Our main findings here are that our carefully gathered compilation of cosmological observations, the largest to date, does not require flat spatial hypersurfaces, with the untitled non-flat Λ CDM inflation model in which spatial curvature contributes about a percent to the current cosmological energy budget being more than 5σ away from flatness; the untitled non-flat model better fits the low- ℓ CMB temperature anisotropy C_ℓ ’s as well as the weak lensing constraints in the σ_8 – Ω_m plane, while the tilted flat- Λ CDM model is more consistent with the higher- ℓ C_ℓ ’s; H_0 is robustly measured in an almost model-independent manner and the value is consistent with most other measurements; and some measured cosmological parameter values, including those of $\Omega_b h^2$, τ , and $\Omega_c h^2$, differ significantly between the two models and so care must be exercised when utilizing cosmological measurements of such parameters.

This paper is organized as follows. In Sec. 2 we describe the cosmological data sets we use in our analyses. In Sec. 3 we summarize the methods we use for our analyses here.

The observational constraints resulting from these data for the tilted flat- Λ CDM and the non-flat Λ CDM inflation models are presented in Sec. 4. We summarize our results in Sec. 5.

2. DATA

2.1. Planck 2015 CMB anisotropy data

We use the Planck 2015 TT + lowP and TT + lowP + lensing CMB anisotropy data (Planck Collaboration 2016). Here TT represents the low- ℓ ($2 \leq \ell \leq 29$) and high- ℓ ($30 \leq \ell \leq 2508$; PlikTT) Planck temperature-only C_ℓ^{TT} data and lowP denotes low- ℓ polarization C_ℓ^{TE} , C_ℓ^{EE} , and C_ℓ^{BB} power spectra measurements at $2 \leq \ell \leq 29$. The collection of low- ℓ temperature and polarization measurements is denoted as lowTEB. For CMB lensing data we use the power spectrum of the lensing potential measured by Planck.

2.2. JLA SNIa data

We use the JLA compilation of 740 SNIa apparent magnitude measurements released by the SDSS-II and SNLS collaborations (Betoule et al. 2014). The JLA data set is composed of several low-redshift SNIa ($z < 0.1$) and higher redshift samples from the SDSS-II ($0.05 < z < 0.4$) and SNLS ($0.2 < z < 1$).

2.3. BAO data

The anisotropy of BAO features in the line-of-sight and the transverse directions enable us to constrain both the Hubble parameter $H(z)$ and the comoving angular diameter distance

$$D_M(z) = (1+z)D_A(z) \quad (1)$$

where D_A is the physical angular diameter distance at redshift z . The radius of the sound horizon at the drag epoch z_d is

$$r_d = \int_{z_d}^{\infty} \frac{c_s(z)}{H(z)} dz \quad (2)$$

where $c_s(z)$ is the sound speed of the photon-baryon fluid. Because the size of the sound horizon r_d depends on the cosmological model and the energy contents, the BAO features in the large-scale structure actually constrain $D_M(z)/r_d$ and $H(z)r_d$.

We use the recent, more reliable BAO distance measurements from the 6dF Galaxy Survey (6dFGS) (Beutler et al. 2011), the Sloan Digital Sky Survey (SDSS) Data Release 7 (DR7) main galaxy sample (MGS) (Ross et al. 2015), the Baryon Oscillation Spectroscopic Survey (BOSS) DR12 galaxies (Alam et al. 2017), the eBOSS DR14 QSO’s (Ata et al. 2018), and the BOSS DR11 and DR12 Ly α forest (Font-Ribera et al. 2014; Bautista et al. 2017), 15 points in total, which are summarized in Table 1.⁵ We call this collection of BAO measurements ‘NewBAO’ to distinguish it from the earlier BAO data compilation (which we call ‘BAO’) of 6dFGS (Beutler et al. 2011), BOSS LOWZ and CMASS (Anderson et al. 2014), and SDSS MGS (Ross et al. 2015) BAO distance measurements, used in the analyses of Planck Collaboration (2016) and Ooba et al. (2018a,b,c).

For BAO data provided by Alam et al. (2017), we include the growth rate ($f\sigma_8$) data in our BAO (and not in our growth rate) analyses here, to be able to properly account for the correlations in the Alam et al. (2017) measurements. For the

⁵ For the BAO data point of Ata et al. (2018) we use the value presented in arXiv:1705.06373v1. In the revised published version (arXiv:1705.06373v2) they updated the data point to $D_V(r_{d,\text{fid}}/r_d) = 3843 \pm 147$ Mpc where $r_{d,\text{fid}}$ is the value of r_d for the fiducial model used in the analysis.

Table 1
BAO measurements.

Data Set	LSS tracers	z_{eff}	Observable	Measurement	Reference
BOSS DR12	galaxies	0.38	$D_M(r_{d,\text{fid}}/r_d)$ [Mpc]	1518 ± 22	Alam et al. (2017)
		0.51	$D_M(r_{d,\text{fid}}/r_d)$ [Mpc]	1977 ± 27	Alam et al. (2017)
		0.61	$D_M(r_{d,\text{fid}}/r_d)$ [Mpc]	2283 ± 32	Alam et al. (2017)
		0.38	$H(r_d/r_{d,\text{fid}})$ [km s ⁻¹ Mpc ⁻¹]	81.5 ± 1.9	Alam et al. (2017)
		0.51	$H(r_d/r_{d,\text{fid}})$ [km s ⁻¹ Mpc ⁻¹]	90.4 ± 1.9	Alam et al. (2017)
		0.61	$H(r_d/r_{d,\text{fid}})$ [km s ⁻¹ Mpc ⁻¹]	97.3 ± 2.1	Alam et al. (2017)
		0.38	$f\sigma_8$	0.497 ± 0.045	Alam et al. (2017)
		0.51	$f\sigma_8$	0.458 ± 0.038	Alam et al. (2017)
		0.61	$f\sigma_8$	0.436 ± 0.034	Alam et al. (2017)
6dF	galaxies	0.106	r_d/D_V	0.327 ± 0.015	Beutler et al. (2011)
SDSS DR7 MGS	galaxies	0.15	$D_V(r_{d,\text{fid}}/r_d)$ [Mpc]	664 ± 25	Ross et al. (2015)
eBOSS DR14	QSOs	1.52	$D_V(r_{d,\text{fid}}/r_d)$ [Mpc]	3855 ± 170	Ata et al. (2018)
BOSS DR12 Ly α forest	Ly α	2.33	$D_H^{0.7} D_M^{0.3}/r_d$	13.94 ± 0.35	Bautista et al. (2017)
BOSS DR11 Ly α forest	QSO & Ly α	2.36	D_H/r_d	9.0 ± 0.3	Font-Ribera et al. (2014)
		2.36	D_A/r_d	10.8 ± 0.4	Font-Ribera et al. (2014)

Note: The sound horizon size of the fiducial model is $r_{d,\text{fid}} = 147.78$ Mpc in Alam et al. (2017) and Ata et al. (2018), and $r_{d,\text{fid}} = 148.69$ Mpc in Ross et al. (2015).

SDSS DR7 MGS (Ross et al. 2015) and BOSS DR11 Ly α forest (Font-Ribera et al. 2014) measurements, we use the probability distributions of the BAO data points, instead of using the Gaussian approximation constraints. Bautista et al. (2017) provide one BAO parameter $D_H^{0.7} D_M^{0.3}/r_d$ at $z = 2.33$ measured from BOSS DR12 Ly α forest observations, where D_H is defined as

$$D_H(z) = c/H(z) \quad (3)$$

where c is the speed of light. Font-Ribera et al. (2014) provide BAO parameters (D_H/r_d and D_A/r_d) measured from the cross-correlation between QSO and Ly α forest data. They actually provide the probability distribution of parameters that describe shifts of the BAO peak position with respect to the fiducial cosmology in perpendicular and parallel directions to the line-of-sight,

$$\alpha_{\perp} = \frac{D_M(z)r_{d,\text{fid}}}{D_M^{\text{fid}}(z)r_d}, \quad \alpha_{\parallel} = \frac{H^{\text{fid}}(z)r_{d,\text{fid}}}{H(z)r_d}. \quad (4)$$

The angle-averaged shift and the ratio of the two α parameters can be converted into the angle-averaged version of the distance scale

$$D_V(z) = [czD_M^2(z)/H(z)]^{1/3}, \quad (5)$$

and the Alcock-Paczynski parameter

$$F_{\text{AP}}(z) = D_M(z)H(z)/c. \quad (6)$$

For the BAO data of Alam et al. (2017), instead of using $D_M(r_{d,\text{fid}}/r_d)$ and $H(r_d/r_{d,\text{fid}})$, we actually transform these into D_V/r_d and F_{AP} and also use their growth rate $f\sigma_8$ measurements and account for correlations (data publicly available at the BOSS website).

2.4. Hubble parameter data

Hubble parameter measurements can be used to constrain dark energy parameters, as well as other cosmological parameters, including the spatial curvature of the Universe (see e.g.,

Farooq et al. 2017).⁶ Here we adapt and use a recent Hubble parameter measurement compilation to constrain both the tilted flat- Λ CDM inflation model and the non-flat Λ CDM inflation model. Table 2 lists all more reliable recent measurements of the Hubble parameter at various redshifts (with 31 data points in total).⁷ See Farooq et al. (2017) and Yu et al. (2018) for discussions about how these data were selected.⁸

2.5. Growth rate data

The growth rate is defined as

$$f(a) = \frac{d \ln D(a)}{d \ln a} \quad (7)$$

where a is the scale factor, $D(a)$ is the amplitude of the matter density perturbation, and $f \approx \Omega_m^{0.55}$ for the Λ CDM model. Information on the growth rate is derived from the peculiar velocities of galaxies. The peculiar velocities can be obtained from the redshift space distortion information imprinted in the large-scale structures of galaxy redshift surveys. The growth rate measurement is sometimes given in terms of $\beta = f/b$, where b is the bias parameter that relates the galaxy density perturbation to the matter one via $\delta_g = b\delta_m$. Since the β parameter strongly depends on the bias parameter, the combination $f(z)\sigma_8(z)$ is more widely used to quantify the growth rate of the matter density perturbation. Here the rms of density

⁶ Early developments include Samushia & Ratra (2006), Samushia et al. (2007), and Chen & Ratra (2011b); recent work includes Tripathi et al. (2017), Lonappan et al. (2017), Rezaei et al. (2017), Magana et al. (2017), Anagnostopoulos & Basilakos (2017), Yu et al. (2018), and Cao et al. (2018). We note that there are many different $H(z)$ compilations discussed in the literature. Unfortunately a significant fraction of these include non-independent or unreliable measurements.

⁷ Table 2 does not list radial or line-of-sight BAO $H(z)$ measurements; these are instead listed in Table 1.

⁸ The redshift range over which the Hubble parameter has been measured encompasses the redshift of the cosmological deceleration-acceleration transition in the standard cosmological model. This transition is between the earlier nonrelativistic-matter-powered decelerating cosmological expansion and the more recent dark-energy-driven accelerating cosmological expansion. This transition redshift has recently been measured and is at roughly the value expected in the standard Λ CDM and other dark energy models (Farooq & Ratra 2013; Moresco et al. 2016; Farooq et al. 2017).

Table 2
Hubble parameter data.

z	$H(z)$ (km s ⁻¹ Mpc ⁻¹)	σ_H (km s ⁻¹ Mpc ⁻¹)	Reference
0.070	69	19.6	Zhang et al. (2014)
0.090	69	12	Simon et al. (2005)
0.120	68.6	26.2	Zhang et al. (2014)
0.170	83	8	Simon et al. (2005)
0.179	75	4	Moresco et al. (2012)
0.199	75	5	Moresco et al. (2012)
0.200	72.9	29.6	Zhang et al. (2014)
0.270	77	14	Simon et al. (2005)
0.280	88.8	36.6	Zhang et al. (2014)
0.352	83	14	Moresco et al. (2012)
0.3802	83	13.5	Moresco et al. (2016)
0.400	95	17	Simon et al. (2005)
0.4004	77	10.2	Moresco et al. (2016)
0.4247	87.1	11.2	Moresco et al. (2016)
0.4497	92.8	12.9	Moresco et al. (2016)
0.47	89	50	Ratsimbazafy et al. (2017)
0.4783	80.9	9	Moresco et al. (2016)
0.480	97	62	Stern et al. (2010)
0.593	104	13	Moresco et al. (2012)
0.680	92	8	Moresco et al. (2012)
0.781	105	12	Moresco et al. (2012)
0.875	125	17	Moresco et al. (2012)
0.880	90	40	Stern et al. (2010)
0.900	117	23	Simon et al. (2005)
1.037	154	20	Moresco et al. (2012)
1.300	168	17	Simon et al. (2005)
1.363	160	33.6	Moresco (2015)
1.430	177	18	Simon et al. (2005)
1.530	140	14	Simon et al. (2005)
1.750	202	40	Simon et al. (2005)
1.965	186.5	50.4	Moresco (2015)

fluctuations within a sphere of $8 h^{-1} \text{Mpc}$ radius is represented by σ_8 for the mass and $\sigma_{8,g}$ for the galaxy distributions. These are related through $\sigma_8 = \sigma_{8,g}/b$ and $f\sigma_8 = \beta\sigma_{8,g}$. The rms mass fluctuation at epoch a is

$$\sigma_8(a) = \sigma_{8,0} \frac{D(a)}{D_0}, \quad (8)$$

where the subscript 0 indicates the present epoch. In the following we denote the present value $\sigma_{8,0}$ as σ_8 for simplicity.

Table 3 lists all more reliable recent measurements of growth rate $f(z)\sigma_8(z)$ at various redshifts, 10 points in total. As already noted, the three growth rate data points of Alam et al. (2017) are included in the collection of BAO data points in order to properly account for correlations between these BAO and growth rate data points.

3. METHODS

3.1. Model computations

We use the publicly available CAMB/COSMOMC package (version of Nov. 2016) (Challinor & Lasenby 1999; Lewis et al. 2000; Lewis & Bridle 2002) to constrain the tilted flat and the non-flat ΛCDM inflation models with Planck 2015 CMB and other non-CMB data sets. The Boltzmann code CAMB computes the CMB angular power spectra for temperature fluctuations, polarization, and lensing potential, and

COSMOMC applies the Markov chain Monte Carlo (MCMC) method to explore and determine model-parameter space that is favored by the data used. We use the COSMOMC settings adopted in the Planck team's analysis (Planck Collaboration 2016). We set the present CMB temperature to $T_0 = 2.7255 \text{ K}$ (Fixsen 2009) and the effective number of neutrino species to $N_{\text{eff}} = 3.046$. We assume the existence of a single species of massive neutrinos with mass $m_\nu = 0.06 \text{ eV}$. The primordial Helium fraction Y_{He} is set from the Big Bang nucleosynthesis prediction. In the parameter estimation the lensed CMB power spectra for each model are compared with observations. When the Planck lensing data are included in the analysis, we also need to consider the non-linear lensing effect that is important in the lensing potential reconstruction (Planck Collaboration 2014). As needed, we turn on the options for CMB lensing and nonlinear lensing in every case, regardless of whether the Planck lensing data are used or not.

The primordial power spectrum in the spatially-flat tilted ΛCDM inflation model (Lucchin & Matarrese 1985; Ratra 1992, 1989) is

$$P(k) = A_s \left(\frac{k}{k_0} \right)^{n_s}, \quad (9)$$

where k is wavenumber and A_s is the amplitude at the pivot scale $k_0 = 0.05 \text{ Mpc}^{-1}$. On the other hand, the primordial power spectrum in the non-flat ΛCDM inflation model (Ratra & Peebles 1995; Ratra 2017) is

$$P(q) \propto \frac{(q^2 - 4K)^2}{q(q^2 - K)}, \quad (10)$$

which goes over to the $n_s = 1$ spectrum in the spatially-flat limit ($K = 0$). For scalar perturbations, $q = \sqrt{k^2 + K}$ is the wavenumber where $K = -(H_0^2/c^2)\Omega_k$ is the spatial curvature. For the spatially-closed model, with negative Ω_k , the normal modes are characterized by the positive integers $\nu = qK^{-1/2} = 3, 4, 5, \dots$, and the eigenvalue of the spatial Laplacian is $-(q^2 - K)/K \equiv -\bar{k}^2/K$. We use $P(q)$ as the initial power spectrum of perturbations for the non-flat model by normalizing its amplitude at the pivot scale k_0 to the value of A_s .

The Planck 2015 non-flat model analyses (Planck Collaboration 2016) are not based on either of the above power spectra, instead they assume

$$P_{\text{Planck}}(q) \propto \frac{(q^2 - 4K)^2}{q(q^2 - K)} \left(\frac{\bar{k}}{k_0} \right)^{n_s-1}, \quad (11)$$

where in addition to the non-flat space wavenumber q , the wavenumber \bar{k} is also used to define and tilt the non-flat model $P_{\text{Planck}}(q)$. The \bar{k}^{n_s-1} tilt factor in $P_{\text{Planck}}(q)$ assumes that tilt in non-flat space works somewhat as it does in flat space, which seems unlikely since spatial curvature sets an additional length scale in non-flat space (i.e., in addition to the Hubble length). It is not known if the power spectrum of Eq. (11) can be the consequence of quantum fluctuations during an early epoch of inflation. This power spectrum is physically sensible if $K = 0$ or if $n_s = 1$, when it reduces to the power spectra in Eqs. (9) and (10), both of which are consequences of quantum fluctuations during inflation.⁹

⁹ Using this expression for the power spectrum (in the seven parameter non-flat ΛCDM model) in analyses of the Planck 2015 data, Planck Collaboration (2016) finds $n_s = 0.9717 \pm 0.0066$ in the TT + lowP case (Planck Collaboration 2015, Table 19.1); since $n_s \neq 1$ it is unclear what significance this result has.

Table 3
Growth rate data.

Data set	z_{eff}	$f(z)\sigma_8(z)$	References	Notes
SNia+IRAS PSCz	0.02	0.398 ± 0.065	Turnbull et al. (2012); Hudson & Turnbull (2012)	$(\Omega_m, \Omega_k) = (0.3, 0)$
2MASS	0.02	0.32 ± 0.04	Springob et al. (2016)	$(\Omega_m, \Omega_k) = (0.308, 0)$
6dFGS	0.067	0.423 ± 0.055	Beutler et al. (2012)	$(\Omega_m, \Omega_k) = (0.27, 0)$
SDSS MGS	0.1	0.37 ± 0.13	Feix et al. (2015)	$(\Omega_m, \Omega_k) = (0.3, 0)$
SDSS MGS	0.15	0.49 ± 0.145	Howlett et al. (2015)	$(\Omega_m, h, \sigma_{8,0}) = (0.31, 0.67, 0.83)$
GAMA	0.18	0.29 ± 0.10	Simpson et al. (2016)	$(\Omega_m, \Omega_k) = (0.27, 0)$
GAMA	0.38	0.44 ± 0.06	Blake et al. (2013)	
VIPERS PDR-2	0.6	0.55 ± 0.12	Pezzotta et al. (2017)	$(\Omega_m, \Omega_b) = (0.3, 0.045)$
VIPERS PDR-2	0.86	0.40 ± 0.11	Pezzotta et al. (2017)	
FastSound	1.4	0.482 ± 0.116	Okumura et al. (2016)	$(\Omega_m, \Omega_k) = (0.27, 0)$

The fiducial models assumed in the analyses are listed in the notes.

3.2. Constraining model parameters

We explore the parameter space of the tilted flat- Λ CDM model with six cosmological parameters ($\Omega_b h^2$, $\Omega_c h^2$, θ_{MC} , τ , A_s , and n_s) and the untilted non-flat Λ CDM model with six parameters ($\Omega_b h^2$, $\Omega_c h^2$, Ω_k , θ_{MC} , τ , and A_s). θ_{MC} is the approximate angular size of the sound horizon (r_*/D_A) at redshift z_* for which the optical depth equals unity (Planck Collaboration 2014). Unresolved extragalactic foregrounds due to point sources, cosmic infrared background, and thermal and kinetic Sunyaev-Zeldovich components contribute to the temperature power spectrum. Thus the foreground model parameters are also constrained as nuisance parameters by the MCMC method. We also compute three derived parameters, H_0 , Ω_m , and σ_8 .

For each model (and set of six parameter values), we compare the lensed CMB power spectra obtained from the CAMB Boltzmann code with the Planck 2015 TT + lowP data and TT + lowP + lensing data, excluding and including the power spectrum of the lensing potential, respectively. For BAO, SNia, and Hubble parameter data, the prediction determined from the spatially homogeneous background evolution equations solution for each set of model parameters is compared with the observations.¹⁰ For growth rate data, the matter density perturbation evolved by the CAMB code is used to compute $f\sigma_8$ at the needed redshifts.

We set priors for some parameters. The Hubble constant is restricted to the range $20 \leq H_0 \leq 100$, in units of $\text{km s}^{-1} \text{Mpc}^{-1}$. The reionization optical depth is explored only in the range $\tau > 0.005$. The other basic parameters have flat priors that are sufficiently wide such that the final constraints are within the prior ranges. For every model considered here sufficient MCMC chains are generated in order that the Gelman and Rubin R statistics satisfy the condition $R \lesssim 0.01$.

4. OBSERVATIONAL CONSTRAINTS

We constrain the spatially-flat tilted and the untilted non-flat Λ CDM inflation models using the Planck 2015 TT + lowP

¹⁰ For parameter estimation using the JLA SNia data set we need to consider hidden nuisance parameters, α_{JLA} and β_{JLA} related to the stretch and color correction of the SNia light curves, B -band absolute magnitude M_B , and the offset of the absolute magnitude due to the environment (host stellar mass) Δ_M . Thus, the number of degrees of freedom for the JLA data is less than the total number of SNia ($N = 740$). For example, for the flat- Λ CDM model that fits the matter density parameter Ω_m , α_{JLA} , β_{JLA} , M_B , and Δ_M , the number of degrees of freedom becomes 735 ($= 740 - 5$). In our analysis, we assume flat priors for these parameters ($0.01 \leq \alpha_{\text{JLA}} \leq 2$ and $0.9 \leq \beta_{\text{JLA}} \leq 4.6$) during parameter estimation.

(excluding and including the CMB lensing) data and other non-CMB data sets.

We first examine how efficient the new BAO data are in constraining parameters, relative to the old BAO data. Figure 1 compares the likelihood distributions of the model parameters for the old ('BAO') and new BAO ('NewBAO') data sets, in conjunction with the CMB observations. The mean and 68.3% confidence limits of model parameters are presented in Table 4. We see that adding CMB lensing data results in a reduction of $\ln(10^{10} A_s)$ and τ in both models and that the NewBAO data improve parameter estimation with slightly narrower parameter constraints (more so for the cases when the lensing data are excluded).

The entries in the TT + lowP + BAO and TT + lowP + lensing + BAO columns for the non-flat Λ CDM model in Table 4 agree well with the corresponding entries in Table 2 of Ooba et al. (2018a). Ooba et al. (2018a) used CLASS (Blas et al. 2011) to compute the C_ℓ 's and Monte Python (Audren et al. 2013) for the MCMC analyses, so it is gratifying and reassuring that our results agree well with those of Ooba et al. (2018a).¹¹

We investigate the effect of including non-CMB data sets, with the Planck 2015 CMB data, on the parameter constraints of the tilted flat and the untilted non-flat Λ CDM models. The results are presented in Figs. 2–5 and Tables 5–8. In the triangle plots we omit the likelihood contours for TT + lowP (+ lensing) + JLA + NewBAO data (excluding or including the Planck lensing data) in both the tilted flat and the untilted non-flat Λ CDM models because they are very similar to those for TT + lowP (+ lensing) + NewBAO data.

The entries in the CMB-only TT + lowP column of Table 5 and those in the TT + lowP + lensing column of Table 6 for the tilted flat- Λ CDM model agree well with the corresponding entries in Table 4 of Planck Collaboration (2016). Similarly, the entries in the TT + lowP column of Table 7 and those in the TT + lowP + lensing column of Table 8 for the non-flat Λ CDM model agree well with the corresponding entries in Table 1 of Ooba et al. (2018a).

From Tables 5 and 6 we see that, when added to the Planck 2015 CMB anisotropy data, for the tilted flat- Λ CDM model, the NewBAO measurements prove more restrictive than either the $H(z)$, $f\sigma_8$, or SNia observations. We note however that our NewBAO compilation includes radial BAO $H(z)$ measure-

¹¹ Note that Ooba et al. (2018a) use CLASS θ that is defined as the ratio of comoving sound horizon to the angular diameter distance at decoupling while here we use CAMB θ_{MC} that is an approximate version of θ .

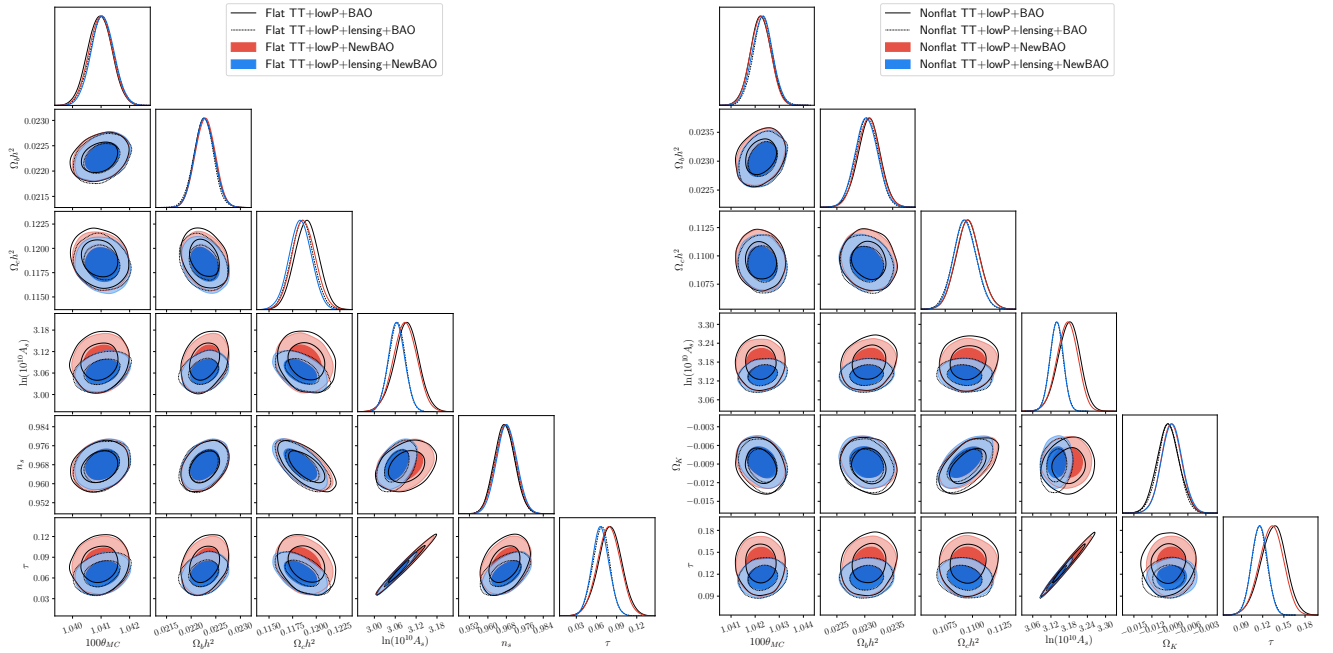


Figure 1. Likelihood distributions of the tilted flat (left) and untilted non-flat (right) Λ CDM model parameters favored by the Planck 2015 CMB TT + lowP (+ lensing) and BAO data. Here the parameter constraints are compared for the old BAO data and the new (NewBAO) data summarized in Table 1. Two-dimensional marginalized likelihood distributions of all possible combinations of model parameters together with one-dimensional likelihoods are shown as solid and dashed black curves for BAO and filled contours and colored curves for NewBAO data.

Table 4
Mean and 68.3% confidence limits of tilted flat and untilted non-flat Λ CDM model parameters. BAO versus NewBAO.

Tilted flat- Λ CDM model				
Parameter	TT+lowP+BAO	TT+lowP+lensing+BAO	TT+lowP+NewBAO	TT+lowP+lensing+NewBAO
$\Omega_b h^2$	0.02227 ± 0.00020	0.02225 ± 0.00020	0.02229 ± 0.00020	0.02227 ± 0.00020
$\Omega_c h^2$	0.1190 ± 0.0013	0.1185 ± 0.0012	0.1187 ± 0.0012	0.1183 ± 0.0012
$100\theta_{MC}$	1.04095 ± 0.00042	1.04103 ± 0.00041	1.04099 ± 0.00041	1.04105 ± 0.00040
τ	0.080 ± 0.018	0.067 ± 0.013	0.079 ± 0.017	0.066 ± 0.013
$\ln(10^{10} A_s)$	3.092 ± 0.035	3.065 ± 0.024	3.088 ± 0.034	3.064 ± 0.024
n_s	0.9673 ± 0.0044	0.9674 ± 0.0044	0.9678 ± 0.0044	0.9682 ± 0.0044
H_0 [km s $^{-1}$ Mpc $^{-1}$]	67.65 ± 0.57	67.81 ± 0.54	67.78 ± 0.55	67.92 ± 0.54
Ω_m	0.3102 ± 0.0076	0.3077 ± 0.0072	0.3083 ± 0.0074	0.3063 ± 0.0071
σ_8	0.829 ± 0.014	0.8158 ± 0.0089	0.826 ± 0.014	0.8150 ± 0.0089
Untilted non-flat Λ CDM model				
Parameter	TT+lowP+BAO	TT+lowP+lensing+BAO	TT+lowP+NewBAO	TT+lowP+lensing+NewBAO
$\Omega_b h^2$	0.02307 ± 0.00020	0.02304 ± 0.00020	0.02307 ± 0.00020	0.02303 ± 0.00020
$\Omega_c h^2$	0.1096 ± 0.0011	0.1093 ± 0.0011	0.1096 ± 0.0011	0.1093 ± 0.0010
$100\theta_{MC}$	1.04222 ± 0.00042	1.04232 ± 0.00041	1.04223 ± 0.00042	1.04230 ± 0.00042
τ	0.135 ± 0.018	0.115 ± 0.011	0.132 ± 0.017	0.115 ± 0.011
$\ln(10^{10} A_s)$	3.179 ± 0.036	3.138 ± 0.022	3.174 ± 0.034	3.139 ± 0.022
Ω_k	-0.0093 ± 0.0019	-0.0093 ± 0.0018	-0.0088 ± 0.0017	-0.0087 ± 0.0017
H_0 [km s $^{-1}$ Mpc $^{-1}$]	67.46 ± 0.72	67.56 ± 0.67	67.69 ± 0.66	67.81 ± 0.66
Ω_m	0.2931 ± 0.0064	0.2914 ± 0.0059	0.2910 ± 0.0059	0.2893 ± 0.0058
σ_8	0.832 ± 0.016	0.814 ± 0.010	0.830 ± 0.015	0.8148 ± 0.0097

ments as well as the $f\sigma_8$ measurements of Alam et al. (2017). It is likely that even if these are moved to the $H(z)$ and $f\sigma_8$ data sets, BAO constraints will still be the most restrictive, for the tilted flat- Λ CDM model, but probably closely followed by $H(z)$ and $f\sigma_8$ constraints, with SNIa being the least effective.

The situation in the untilted non-flat Λ CDM case is more interesting. When CMB lensing data are excluded, Table 7, adding NewBAO, or JLA SNIa, or $H(z)$, or $f\sigma_8$ data to the CMB data results in roughly similarly restrictive constraints on $\Omega_b h^2$, $\Omega_c h^2$, θ_{MC} , τ , $\ln(10^{10} A_s)$, and σ_8 , while CMB + NewBAO data provide the tightest constraints on Ω_k , H_0 , and Ω_m . When the CMB lensing data are included, Table 8, CMB data with either JLA SNIa, or NewBAO, or $H(z)$, or $f\sigma_8$ data, provide roughly similarly restrictive constraints on $\Omega_b h^2$, $\Omega_c h^2$, and θ_{MC} , while CMB + NewBAO data provide the tightest constraints on τ , $\ln(10^{10} A_s)$, Ω_k , H_0 , Ω_m , and σ_8 .

If we focus on CMB TT + lowP + lensing data, Figs. 3 and 5 and Tables 6 and 8, we see that adding only one of the four non-CMB data sets at a time to the CMB measurements (left triangle plots in the two figures) results in four sets of contours that are quite consistent with each other, as well as with the original CMB alone contours, for both the tilted flat- Λ CDM case and for the untilted non-flat Λ CDM model. The same holds true for the tilted flat- Λ CDM model when the CMB lensing data are excluded (left triangle plot of Fig. 2). However, in the untilted non-flat Λ CDM case without the lensing data when any of the four non-CMB data sets are added to the CMB data (left triangle plot of Fig. 4), they each pull the results towards a smaller $|\Omega_k|$ (closer to the flat model) and slightly larger τ and $\ln(10^{10} A_s)$ and smaller $\Omega_b h^2$ than is favored by the CMB data alone, although all five sets of constraint contours are largely mutually consistent. It is reassuring that the four non-CMB data sets do not pull the CMB constraints in significantly different directions.

As noted above, adding the NewBAO data to the CMB data typically makes the biggest difference, but the other three non-CMB data sets also contribute. Focusing on the TT + lowP + lensing data, we see from Table 6 for the tilted flat- Λ CDM case that the NewBAO data tightly constrains model parameters, particularly $\Omega_c h^2$, while the growth rate ($f\sigma_8$) data shifts $\Omega_b h^2$ and n_s to larger values and $\Omega_c h^2$ to a smaller value. In this case Ω_m is the quantity whose error bar is reduced the most by the full combination of data relative to the CMB and NewBAO compilation, followed by the H_0 error bar reduction. For the untilted non-flat Λ CDM model, from Table 8, $\Omega_c h^2$ and τ error bars from the CMB and NewBAO data are not reduced by including the $H(z)$, $f\sigma_8$, and JLA SNIa measurements in the mix. In all cases, adding JLA SNIa or growth rate ($f\sigma_8$) data to the combination of CMB + NewBAO data does not much improve the observational constraints.¹²

Again concentrating on the TT + lowP + lensing data, Tables 6 and 8, we see that for the tilted flat- Λ CDM model, adding the four non-CMB data sets to the mix most affects $\Omega_c h^2$ and Ω_m , with both central values moving down about 0.5σ of the CMB data alone error bars. The situation in the untilted non-flat Λ CDM case is a little more dramatic, with Ω_k moving closer to flatness by about 1σ , H_0 and Ω_m also moving by about 1σ , and the σ_8 , $\ln(10^{10} A_s)$, and τ central values moving by about 0.5σ .

Perhaps the biggest consequence of including the four non-

CMB data sets in the analyses is the significant strengthening of the evidence for non-flatness in the untilted non-flat Λ CDM case, with it increasing from 1.8σ away from flatness for the CMB alone case, to 5.1σ away from flatness for the full data combination in Table 8,¹³ where the NewBAO data plays the most important role among the four non-CMB data sets. This is consistent with, but stronger than, the Ooba et al. (2018a) results. The same situation is also seen when the lensing data are excluded, as shown in Table 7. We also note that combining CMB data with either JLA SNIa, $H(z)$, or growth rate data do not strongly support non-flatness. When combined with CMB data with lensing, SNIa, $H(z)$, and $f\sigma_8$ data result in Ω_k being 2.1σ , 1.8σ , and 1.2σ away from flatness, while CMB and NewBAO data favor Ω_k being 5.1σ away from flatness (Table 8). In the untilted non-flat Λ CDM case, the effect of growth rate data on the model constraints differs from that of the NewBAO data. The results for the untilted non-flat Λ CDM model from TT + lowP + $f\sigma_8$ observations excluding (including) the lensing data shows that the growth rate measurements favor Ω_k moving closer to spatial flatness with a deviation of only 1.4σ (1.2σ) from zero spatial curvature. Adding $f\sigma_8$ data to TT + lowP (+ lensing) + NewBAO measurements — that favor the closed model by 5.2σ (5.1σ) — gives a negative Ω_k deviating from flatness by 5.1σ (5.1σ). Thus the negativeness of the curvature parameter persists for the combination of BAO and growth rate data, which also implies that the BAO data most tightly constrains the curvature parameter compared to the other non-CMB data.

For the full data combination, H_0 measured in the two models (with lensing data) in Tables 6 and 8, 68.17 ± 0.50 and 68.07 ± 0.63 km s⁻¹ Mpc⁻¹, are very consistent with each other, agreeing to within 0.12σ (of the quadrature sum of the two error bars).¹⁴ These values are consistent with the most recent median statistics estimate $H_0 = 68 \pm 2.8$ km s⁻¹ Mpc⁻¹ (Chen & Ratra 2011a), which is consistent with earlier median statistics estimates (Gott et al. 2001; Chen et al. 2003). Many recent estimates of H_0 are also quite consistent with these measurements (Calabrese et al. 2012; Hinshaw et al. 2013; Sievers et al. 2013; Aubourg et al. 2015; Planck Collaboration 2016; L’Huillier & Shafieloo 2017; Chen et al. 2017; Luković et al. 2016; Wang et al. 2017; Lin & Ishak 2017; DES Collaboration 2017b; Yu et al. 2018; Haridasu et al. 2018), but, as is well known, they are lower than the local measurement of $H_0 = 73.06 \pm 1.74$ km s⁻¹ Mpc⁻¹ (Anderson & Riess 2017).¹⁵

In our analyses here, H_0 and σ_8 (discussed below) are the only cosmological parameters that are determined in a cosmological model (spatial curvature and tilt) independent manner. For instance, Ω_m determined using the tilted flat- Λ CDM model differs from that measured in the untilted non-flat Λ CDM model by about 1.9σ (of the quadrature sum of the error bars), however both estimates are consistent with many other determinations (see e.g., Chen & Ratra 2003).

Like Ω_m , measurements of θ_{MC} , $\Omega_b h^2$, $\ln(10^{10} A_s)$, and τ

¹³ It is possible to assume that all one-dimensional likelihoods are close to Gaussian, except for Ω_k estimated using the TT + lowP, TT + lowP + $H(z)$, and TT + lowP + $f\sigma_8$ data.

¹⁴ Potential systematic errors, ignored here, have been discussed by Addison et al. (2016) and Planck Collaboration (2017).

¹⁵ This local measurement is 2.7σ (of the quadrature sum of the two error bars) higher than H_0 measured in both models. We note that some other local expansion rate measurements find a slightly lower H_0 with larger error bars (Rigault et al. 2015; Zhang et al. 2017; Dhawan et al. 2018; Fernández Arenas et al. 2018).

¹² We did not check what happens when just $H(z)$ data is added to the CMB and NewBAO combination but suspect a similar conclusion holds for this case also.

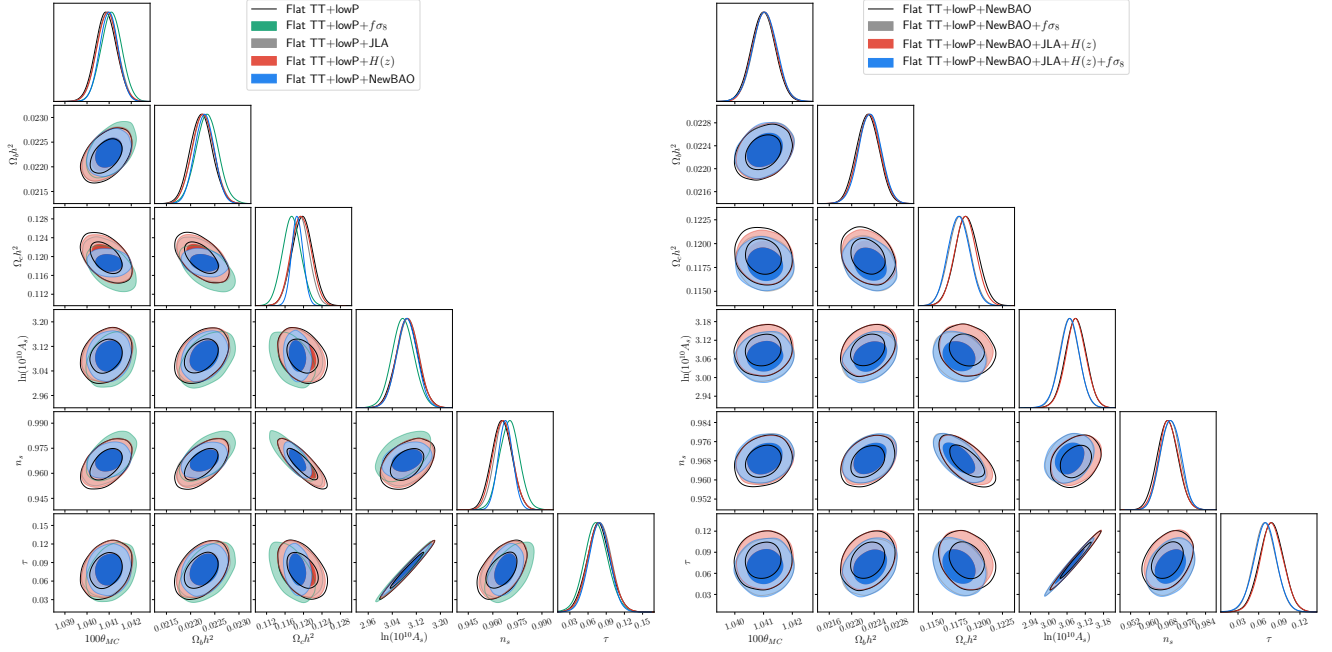


Figure 2. Likelihood distributions of the tilted flat- Λ CDM model parameters constrained by Planck CMB TT + lowP, JLA SNIa, NewBAO, $H(z)$, and $f\sigma_8$ data. Two-dimensional marginalized likelihood distributions of all possible combinations of model parameters together with one-dimensional likelihoods are shown for cases when each non-CMB data set is added to the Planck TT + lowP data (left panel) and when the growth rate, JLA SNIa, Hubble parameter data, and the combination of them, are added to TT + lowP + NewBAO data (right panel). For ease of viewing, the cases of TT + lowP (left) and TT + lowP + NewBAO (right panel) are shown as solid black curves.

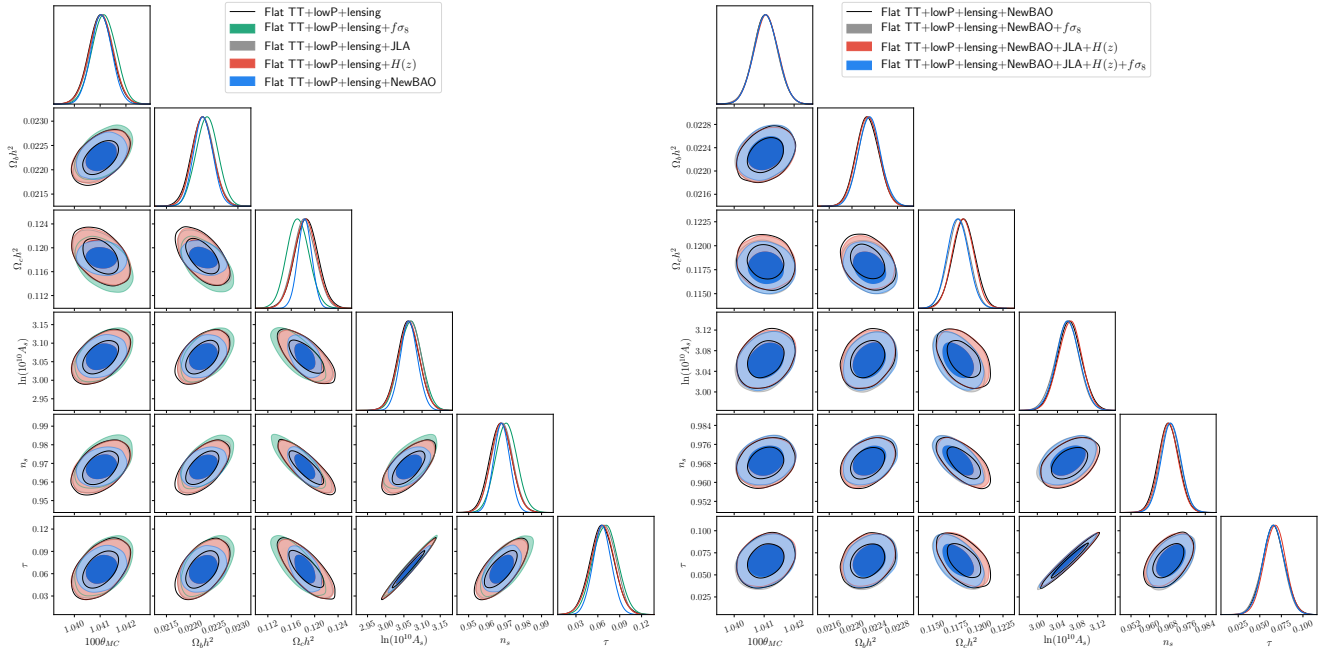


Figure 3. Same as Fig. 2 but now including the Planck CMB lensing data.

are more model dependent, differing by 2.1σ , 2.3σ , 2.7σ , and 2.9σ between the two models. The measurements of $\Omega_c h^2$ differ by 5.7σ , so the cosmological model dependence of this measurement is much more important than the statistical errors determined by using a given cosmological model. It is important to account for such model dependence when comparing a cosmologically estimated value to that estimated using a different technique. This model dependence can have

very striking consequences. For instance, as discussed in [Mitra et al. \(2018, 2019\)](#), the much larger value of τ in the untilted non-flat case significantly alters the cosmological reionization scenario, although we note that using the more extensive non-CMB data compilation here we find a 0.6σ reduction in τ compared to the larger value found in [Ooba et al. \(2018a\)](#) thus somewhat alleviating the potential tension discovered in [Mitra et al. \(2018, 2019\)](#) for the higher τ

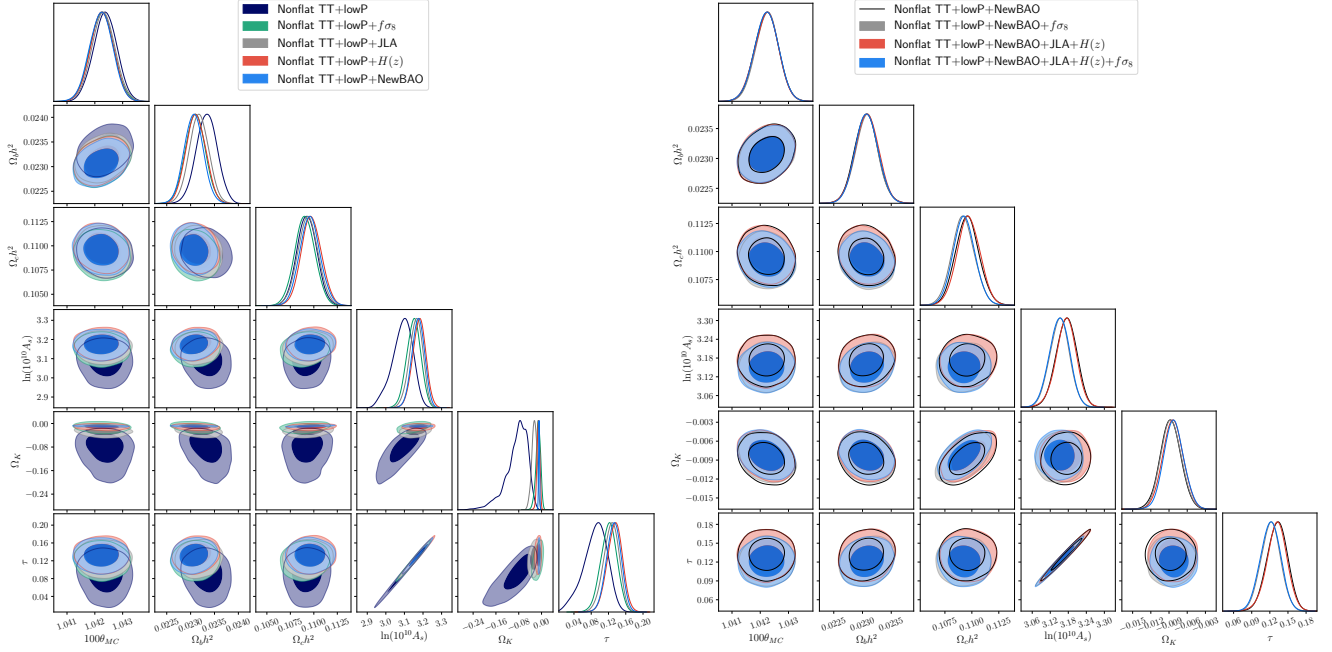


Figure 4. Likelihood distributions of the untilted non-flat Λ CDM model parameters constrained by Planck CMB TT + lowP, JLA SNIa, NewBAO, $H(z)$, and $f\sigma_8$ data. Two-dimensional marginalized likelihood distributions of all possible combinations of model parameters together with one-dimensional likelihoods are shown for cases when each non-CMB data set is added to the Planck TT + lowP data (left panel) and when the growth rate, JLA SNIa, Hubble parameter data, and the combination of them, are added to TT + lowP + NewBAO data (right panel). For ease of viewing, the result of TT + lowP + NewBAO is shown as solid black curves in the right panel.

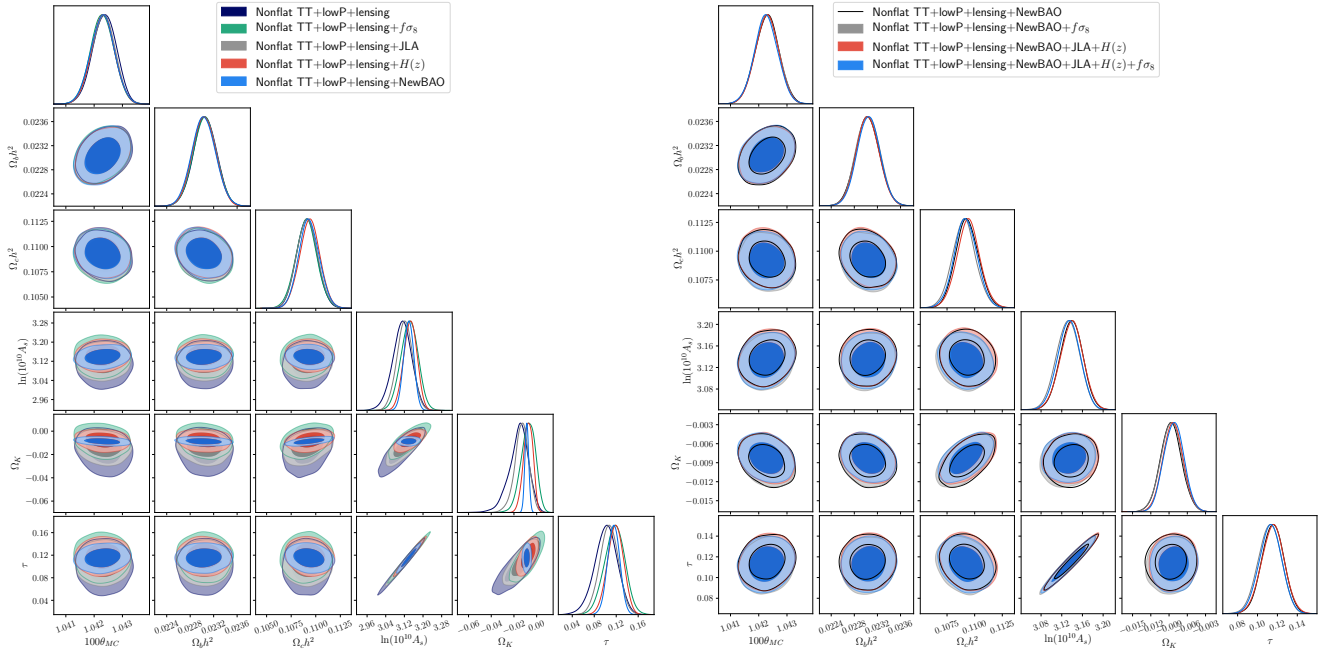


Figure 5. Same as Fig. 4 but now including the Planck CMB lensing data.

value. From Tables 6 and 8, for the full data compilation including CMB lensing observations, we find in the tilted flat- Λ CDM (non-flat Λ CDM) model $0.02193 \leq \Omega_b h^2 \leq 0.02269$ ($0.02265 \leq \Omega_b h^2 \leq 0.02345$) at 2σ , which are almost disjoint.¹⁶ Clearly it is not possible to robustly measure $\Omega_b h^2$

¹⁶ A compilation of measured primordial deuterium abundances mildly favors the flat case (Penton et al. 2018).

(and some other cosmological parameters) in a model independent way from cosmological data and care must be taken when comparing a value measured in a cosmological model to a value determined using some other technique (see, e.g. Cooke et al. 2018).

For the full data combination, σ_8 's measured in the two models (with CMB lensing data), Tables 6 and 8, agree to 0.062σ (of the quadrature sum of the two error bars). Fig-

Table 5Tilted flat- Λ CDM model parameters constrained with Planck TT + lowP, JLA SNIa, NewBAO, $H(z)$, and $f\sigma_8$ data (mean and 68.3% confidence limits).

Parameter	TT+lowP	TT+lowP+JLA	TT+lowP+NewBAO
$\Omega_b h^2$	0.02222 ± 0.00023	0.02226 ± 0.00022	0.02229 ± 0.00020
$\Omega_c h^2$	0.1197 ± 0.0022	0.1193 ± 0.0020	0.1187 ± 0.0012
$100\theta_{\text{MC}}$	1.04086 ± 0.00048	1.04092 ± 0.00047	1.04099 ± 0.00041
τ	0.078 ± 0.019	0.080 ± 0.019	0.079 ± 0.017
$\ln(10^{10} A_s)$	3.089 ± 0.037	3.092 ± 0.035	3.088 ± 0.034
n_s	0.9655 ± 0.0062	0.9666 ± 0.0057	0.9678 ± 0.0044
H_0 [km s $^{-1}$ Mpc $^{-1}$]	67.32 ± 0.99	67.52 ± 0.89	67.78 ± 0.55
Ω_m	0.315 ± 0.014	0.312 ± 0.012	0.3083 ± 0.0074
σ_8	0.829 ± 0.015	0.829 ± 0.014	0.826 ± 0.014
Parameter	TT+lowP+ $H(z)$	TT+lowP+JLA+NewBAO	TT+lowP+JLA+NewBAO+ $H(z)$
$\Omega_b h^2$	0.02225 ± 0.00022	0.02230 ± 0.00019	0.02231 ± 0.00020
$\Omega_c h^2$	0.1195 ± 0.0021	0.1186 ± 0.0012	0.1185 ± 0.0012
$100\theta_{\text{MC}}$	1.04091 ± 0.00047	1.04101 ± 0.00041	1.04103 ± 0.00041
τ	0.079 ± 0.019	0.078 ± 0.017	0.079 ± 0.017
$\ln(10^{10} A_s)$	3.091 ± 0.036	3.088 ± 0.034	3.089 ± 0.034
n_s	0.9661 ± 0.0060	0.9679 ± 0.0044	0.9682 ± 0.0042
H_0 [km s $^{-1}$ Mpc $^{-1}$]	67.44 ± 0.94	67.82 ± 0.55	67.85 ± 0.52
Ω_m	0.313 ± 0.013	0.3078 ± 0.0072	0.3074 ± 0.0068
σ_8	0.829 ± 0.014	0.826 ± 0.014	0.826 ± 0.014
Parameter	TT+lowP+ $f\sigma_8$	TT+lowP+NewBAO+ $f\sigma_8$	TT+lowP+JLA+NewBAO+ $H(z)$ + $f\sigma_8$
$\Omega_b h^2$	0.02234 ± 0.00023	0.02231 ± 0.00020	0.02232 ± 0.00020
$\Omega_c h^2$	0.1174 ± 0.0020	0.1179 ± 0.0012	0.1178 ± 0.0011
$100\theta_{\text{MC}}$	1.04110 ± 0.00046	1.04104 ± 0.00041	1.04104 ± 0.00042
τ	0.074 ± 0.020	0.069 ± 0.016	0.069 ± 0.017
$\ln(10^{10} A_s)$	3.076 ± 0.037	3.068 ± 0.032	3.068 ± 0.033
n_s	0.9702 ± 0.0061	0.9689 ± 0.0042	0.9690 ± 0.0043
H_0 [km s $^{-1}$ Mpc $^{-1}$]	68.31 ± 0.94	68.09 ± 0.54	68.12 ± 0.52
Ω_m	0.301 ± 0.012	0.3040 ± 0.0069	0.3035 ± 0.0067
σ_8	0.817 ± 0.014	0.815 ± 0.013	0.815 ± 0.013

ures 6 and 7 show the marginalized two-dimensional likelihood distribution of Ω_m and σ_8 for the tilted flat and untilted non-flat Λ CDM models constrained by the Planck CMB and the non-CMB data sets. For comparison, in each panel we present the Λ CDM constraints obtained from a combined analysis of galaxy clustering and weak gravitational lensing based on the first year result of the Dark Energy Survey (DES Y1 All) (DES Collaboration 2017a), whose 68.3% confidence limits are $\Omega_m = 0.264^{+0.032}_{-0.019}$ and $\sigma_8 = 0.807^{+0.062}_{-0.041}$. The likelihood distribution in the Ω_m - σ_8 plane obtained by adding each non-CMB data set to the Planck CMB data are consistent with each other. As expected, the NewBAO data or the NewBAO data combined with other non-CMB data sets give tighter constraints in all cases. As shown in Figs. 6 and 7, there is tension between both Λ CDM models constrained by Planck TT + lowP data (dotted and dashed curves in the top panels) and the DES constraints. This tension disappears when the CMB lensing data are included (bottom panels).

Although our σ_8 constraints from the flat and non-flat models (excluding and including CMB lensing data) are similar to the DES Y1 All result, our Ω_m constraints favor a larger value by over 1σ for the flat- Λ CDM model. Including the CMB lensing data reduces the tension to 1.2σ . We note that the best-fit point for the non-flat Λ CDM model constrained

by the Planck CMB data (including lensing) combined with all non-CMB data enters well into the 1σ region of the DES Y1 All constraint contour (Fig. 7 lower right panel), unlike the case for the tilted flat- Λ CDM model (Fig. 6 lower right panel).

Table 9 lists the individual and total χ^2 values for the best-fit tilted flat and untilted non-flat Λ CDM models. The best-fit position in the parameter space is found with the COSMOMC built-in routine that obtains the minimum χ^2 by using Powell's minimization method. This method searches for the local minimum by differentiating the likelihood distribution and is efficient at finding the accurate location of the minimum χ^2 .¹⁷ We present the individual contribution of each data set used to constrain the model parameters. The total χ^2 is the sum of those from the high- ℓ CMB TT likelihood (χ^2_{PlikTT}), the low- ℓ CMB power spectra (χ^2_{lowTEB}), lensing (χ^2_{lensing}), JLA SNIa (χ^2_{JLA}), NewBAO (χ^2_{NewBAO}), $H(z)$ ($\chi^2_{H(z)}$), $f\sigma_8$ data ($\chi^2_{f\sigma_8}$), and the contribution from the foreground nuisance parameters (χ^2_{prior}). The nonstandard normalization of the Planck 2015 CMB data likelihoods means that only the difference of χ^2 of

¹⁷ Our minimum χ^2 values are very similar to those supplied by the Planck team. For the tilted flat- Λ CDM model constrained with TT + lowP data, the Planck team provides χ^2 estimated from Powell's minimization method: $\chi^2_{\text{Plik}} = 763.37$, $\chi^2_{\text{lowTEB}} = 10496.47$, $\chi^2_{\text{prior}} = 2.08$, with total $\chi^2 = 11261.9$.

Table 6Tilted flat- Λ CDM model parameters constrained with Planck TT + lowP + lensing, JLA, NewBAO, $H(z)$, and $f\sigma_8$ data (mean and 68.3% confidence limits).

Parameter	TT+lowP+lensing	TT+lowP+lensing+JLA	TT+lowP+lensing+NewBAO
$\Omega_b h^2$	0.02225 ± 0.00023	0.02227 ± 0.00022	0.02227 ± 0.00020
$\Omega_c h^2$	0.1186 ± 0.0020	0.1183 ± 0.0019	0.1183 ± 0.0012
$100\theta_{MC}$	1.04102 ± 0.00046	1.04105 ± 0.00045	1.04105 ± 0.00040
τ	0.066 ± 0.017	0.068 ± 0.016	0.066 ± 0.013
$\ln(10^{10} A_s)$	3.063 ± 0.030	3.066 ± 0.029	3.064 ± 0.024
n_s	0.9677 ± 0.0060	0.9683 ± 0.0058	0.9682 ± 0.0044
H_0 [km s $^{-1}$ Mpc $^{-1}$]	67.80 ± 0.92	67.93 ± 0.88	67.92 ± 0.54
Ω_m	0.308 ± 0.012	0.306 ± 0.012	0.3063 ± 0.0071
σ_8	0.8151 ± 0.0095	0.8156 ± 0.0093	0.8150 ± 0.0089
Parameter	TT+lowP+lensing+ $H(z)$	TT+lowP+lensing+JLA+NewBAO	TT+lowP+lensing+JLA+NewBAO+ $H(z)$
$\Omega_b h^2$	0.02226 ± 0.00022	0.02227 ± 0.00020	0.02228 ± 0.00019
$\Omega_c h^2$	0.1184 ± 0.0019	0.1182 ± 0.0011	0.1182 ± 0.0011
$100\theta_{MC}$	1.04104 ± 0.00046	1.04105 ± 0.00040	1.04107 ± 0.00040
τ	0.066 ± 0.016	0.067 ± 0.013	0.067 ± 0.012
$\ln(10^{10} A_s)$	3.063 ± 0.029	3.064 ± 0.024	3.064 ± 0.023
n_s	0.9680 ± 0.0058	0.9682 ± 0.0043	0.9682 ± 0.0043
H_0 [km s $^{-1}$ Mpc $^{-1}$]	67.86 ± 0.88	67.95 ± 0.52	67.95 ± 0.51
Ω_m	0.307 ± 0.012	0.3058 ± 0.0068	0.3058 ± 0.0067
σ_8	0.8151 ± 0.0094	0.8149 ± 0.0090	0.8149 ± 0.0089
Parameter	TT+lowP+lensing+ $f\sigma_8$	TT+lowP+lensing+NewBAO+ $f\sigma_8$	TT+lowP+lensing+JLA+NewBAO+ $H(z)$ + $f\sigma_8$
$\Omega_b h^2$	0.02235 ± 0.00023	0.02230 ± 0.00020	0.02231 ± 0.00019
$\Omega_c h^2$	0.1171 ± 0.0019	0.1178 ± 0.0011	0.1177 ± 0.0011
$100\theta_{MC}$	1.04115 ± 0.00046	1.04104 ± 0.00041	1.04106 ± 0.00040
τ	0.070 ± 0.017	0.065 ± 0.013	0.066 ± 0.012
$\ln(10^{10} A_s)$	3.068 ± 0.030	3.059 ± 0.024	3.061 ± 0.023
n_s	0.9707 ± 0.0059	0.9690 ± 0.0043	0.9692 ± 0.0042
H_0 [km s $^{-1}$ Mpc $^{-1}$]	68.44 ± 0.89	68.13 ± 0.52	68.17 ± 0.50
Ω_m	0.299 ± 0.011	0.3033 ± 0.0068	0.3027 ± 0.0065
σ_8	0.8130 ± 0.0094	0.8113 ± 0.0087	0.8116 ± 0.0087

one model relative to the other is meaningful for the Planck CMB data. In Table 9, for the untilted non-flat Λ CDM model, we list $\Delta\chi^2$, the excess χ^2 over the value of the tilted flat- Λ CDM model constrained with the same combination of data sets. For the non-CMB data sets, the numbers of degrees of freedom are 735, 15, 31, 10 for JLA SNIa, NewBAO, $H(z)$, $f\sigma_8$ data sets, respectively, for a total of 791 degrees of freedom. The reduced χ^2 's for the individual non-CMB data sets are $\chi^2/\nu \lesssim 1$. There are 189 points in the TT + lowP Planck 2015 data (binned angular power spectrum) and 197 when the CMB lensing observations are included.

Let us first focus on how the model fits the individual data sets. Compared to the tilted flat- Λ CDM model, the untilted non-flat Λ CDM model constrained with the Planck CMB data alone (excluding and including CMB lensing data) does worse at fitting the Planck high- ℓ C_ℓ 's while it fits the low- ℓ ones a bit better. Inclusion of the non-CMB data with the CMB data also results in the best-fit untilted non-flat model providing a poorer fit to the high- ℓ TT measurements, both with and without the lensing data, compared to the tilted flat- Λ CDM case. Adding JLA SNIa or NewBAO data to the Planck TT + lowP + lensing data improves the untilted non-flat model fit to the Planck low- ℓ TEB data. There is a tendency for the non-flat models to more poorly fit the NewBAO and $H(z)$ data

(with larger values of χ^2_{NewBAO} and $\chi^2_{H(z)}$) than the flat models do, while the opposite is true for the case of the growth rate ($f\sigma_8$) measurements.

Comparing results for the TT + lowP + lensing analyses, $\Delta\chi^2 = 21$ for the full data compilation, for the non-flat Λ CDM case relative to the flat- Λ CDM model (last column in the last row of Table 9). Unfortunately it is unclear how to turn this into a quantitative relative probability as the two six parameter models are not nested (and the number of degrees of freedom of the Planck CMB anisotropy data is not available). Rather the best-fit versions of each six parameter model provide distinct local likelihood maxima in a larger seven parameter model space.¹⁸ However, it is clear that the untilted non-flat Λ CDM model does not do as good a job in fitting the higher- ℓ C_ℓ 's as it does in fitting the lower- ℓ ones. In this context it might be relevant to note that there has been some discussion about systematic differences between constraints derived using the higher- ℓ and the lower- ℓ Planck 2015 CMB data (Addison et al. 2016; Planck Collaboration 2017). Additionally, in the flat- Λ CDM model, there appear to be inconsistencies between the higher- ℓ Planck 2015 CMB anisotropy data and the South Pole Telescope CMB anisotropy data (Ay-

¹⁸ The energy density inhomogeneity power spectrum for this seven parameter tilted non-flat Λ CDM model is not known.

Table 7

Untilted non-flat Λ CDM model parameters constrained with Planck TT + lowP, JLA SNIa, NewBAO, $H(z)$, and $f\sigma_8$ data (mean and 68.3% confidence limits).

Parameter	TT+lowP	TT+lowP+JLA	TT+lowP+NewBAO
$\Omega_b h^2$	0.02334 ± 0.00022	0.02318 ± 0.00020	0.02307 ± 0.00020
$\Omega_c h^2$	0.1093 ± 0.0011	0.1094 ± 0.0011	0.1096 ± 0.0011
$100\theta_{MC}$	1.04237 ± 0.00042	1.04231 ± 0.00042	1.04223 ± 0.00042
τ	0.089 ± 0.028	0.126 ± 0.018	0.132 ± 0.017
$\ln(10^{10} A_s)$	3.088 ± 0.055	3.162 ± 0.036	3.174 ± 0.034
Ω_k	-0.088 ± 0.040	-0.0257 ± 0.0091	-0.0088 ± 0.0017
H_0 [km s $^{-1}$ Mpc $^{-1}$]	49.1 ± 5.4	61.5 ± 2.9	67.69 ± 0.66
Ω_m	0.58 ± 0.14	0.355 ± 0.033	0.2910 ± 0.0059
σ_8	0.755 ± 0.038	0.815 ± 0.018	0.830 ± 0.015
Parameter	TT+lowP+ $H(z)$	TT+lowP+JLA+NewBAO	TT+lowP+JLA+NewBAO+ $H(z)$
$\Omega_b h^2$	0.02311 ± 0.00020	0.02307 ± 0.00020	0.02308 ± 0.00020
$\Omega_c h^2$	0.1097 ± 0.0011	0.1096 ± 0.0011	0.1097 ± 0.0011
$100\theta_{MC}$	1.04225 ± 0.00041	1.04223 ± 0.00040	1.04222 ± 0.00042
τ	0.134 ± 0.018	0.132 ± 0.016	0.132 ± 0.017
$\ln(10^{10} A_s)$	3.179 ± 0.036	3.173 ± 0.032	3.172 ± 0.034
Ω_k	-0.0113 ± 0.0051	-0.0087 ± 0.0016	-0.0084 ± 0.0017
H_0 [km s $^{-1}$ Mpc $^{-1}$]	66.7 ± 2.2	67.69 ± 0.63	67.85 ± 0.65
Ω_m	0.302 ± 0.020	0.2910 ± 0.0057	0.2899 ± 0.0058
σ_8	0.831 ± 0.016	0.830 ± 0.014	0.830 ± 0.015
Parameter	TT+lowP+ $f\sigma_8$	TT+lowP+NewBAO+ $f\sigma_8$	TT+lowP+JLA+NewBAO+ $H(z)$ + $f\sigma_8$
$\Omega_b h^2$	0.02310 ± 0.00021	0.02307 ± 0.00019	0.02307 ± 0.00020
$\Omega_c h^2$	0.1090 ± 0.0011	0.1092 ± 0.0010	0.1093 ± 0.0010
$100\theta_{MC}$	1.04225 ± 0.00042	1.04224 ± 0.00040	1.04222 ± 0.00042
τ	0.121 ± 0.019	0.121 ± 0.016	0.121 ± 0.017
$\ln(10^{10} A_s)$	3.150 ± 0.038	3.151 ± 0.032	3.151 ± 0.033
Ω_k	-0.0120 ± 0.0085	-0.0087 ± 0.0017	-0.0082 ± 0.0016
H_0 [km s $^{-1}$ Mpc $^{-1}$]	66.8 ± 3.6	67.87 ± 0.64	68.04 ± 0.62
Ω_m	0.301 ± 0.032	0.2886 ± 0.0057	0.2874 ± 0.0055
σ_8	0.816 ± 0.019	0.819 ± 0.014	0.820 ± 0.014

lor et al. 2017).

To compare untitled non-flat Λ CDM model with the tilted flat one, we may also use the Bayes factor $B = E[\text{nonflat}]/E[\text{flat}]$ that is defined as a ratio of Bayesian evidence of non-flat model relative to the flat one for the same combination of data sets. The Bayesian evidence of a model M is given by

$$E = p(x|M) = \int d\theta p(x|\theta, M) \pi(\theta|M), \quad (12)$$

where x indicates a data set, θ is a vector containing parameters of the model M , and $\pi(\theta|M)$ is the prior on the parameters. We calculate the Bayesian evidence using the algorithm developed by Heavens et al. (2017) in which the posterior for the Bayesian evidence is obtained with the nearest-neighbor distances in parameter space. In Table 9 we list the logarithm of Bayes factor $\ln B$ for each untitled non-flat Λ CDM model relative to the tilted flat one. In all cases, we find that $\ln B < -5$, which indicates very strong evidence that the untitled non-flat Λ CDM model is less favored than the tilted flat one (Trotta 2008). However, we again take note of possible systematic differences in the CMB data mentioned at the end of the previous paragraph (Addison et al. 2016; Planck Collaboration 2017; Aylor et al. 2017) which, if real, could alter the Bayesian evidence in either direction. In addition, the

Bayesian evidence we have computed here does not account for the fact that the best-fit untitled non-flat model has a lower Ω_m than does the best-fit tilted flat model (when both are fit to the cosmological data compilation we have used in our analyses here), and so is in better agreement with the lower Ω_m determined from weak-lensing measurements.

Figures 8 and 9 show the CMB high- ℓ TT, and the low- ℓ TT, TE, EE power spectra of the best-fit tilted flat and untitled non-flat Λ CDM models, excluding and including the lensing data, respectively. The non-flat Λ CDM model constrained by adding each non-CMB data set to the Planck 2015 CMB anisotropy observations generally gives a poorer fit to the low- ℓ EE power spectrum while it better fits the low- ℓ TT power spectrum (see the bottom left panel of Figs. 8 and 9). The shape of the best-fit C_ℓ power spectra of various models relative to the Planck CMB data points are consistent with the χ^2 values listed in Table 9.

Figure 10 shows the best-fit initial power spectra of scalar-type fractional energy density perturbations for the non-flat Λ CDM model constrained by the Planck TT + lowP (left) and TT + lowP + lensing (right panel) data together with other non-CMB data sets. The reduction in power at low q in the best-fit closed- Λ CDM inflation model power spectra shown in Fig. 10 is partially responsible for the low- ℓ TT power re-

Table 8

Untilted non-flat Λ CDM model parameters constrained with Planck TT + lowP + lensing, JLA, NewBAO, $H(z)$, and $f\sigma_8$ data (mean and 68.3% confidence limits).

Parameter	TT+lowP+lensing	TT+lowP+lensing+JLA	TT+lowP+lensing+NewBAO
$\Omega_b h^2$	0.02305 ± 0.00020	0.02304 ± 0.00020	0.02303 ± 0.00020
$\Omega_c h^2$	0.1091 ± 0.0010	0.1091 ± 0.0011	0.1093 ± 0.0010
$100\theta_{MC}$	1.04237 ± 0.00042	1.04233 ± 0.00041	1.04230 ± 0.00042
τ	0.101 ± 0.021	0.107 ± 0.017	0.115 ± 0.011
$\ln(10^{10} A_s)$	3.110 ± 0.041	3.120 ± 0.034	3.139 ± 0.022
Ω_k	-0.0160 ± 0.0087	-0.0133 ± 0.0063	-0.0087 ± 0.0017
H_0 [km s $^{-1}$ Mpc $^{-1}$]	65.1 ± 3.3	66.0 ± 2.5	67.81 ± 0.66
Ω_m	0.316 ± 0.033	0.306 ± 0.023	0.2893 ± 0.0057
σ_8	0.799 ± 0.021	0.805 ± 0.017	0.8148 ± 0.0097
Parameter	TT+lowP+lensing+ $H(z)$	TT+lowP+lensing+JLA+NewBAO	TT+lowP+lensing+JLA+NewBAO+ $H(z)$
$\Omega_b h^2$	0.02304 ± 0.00020	0.02302 ± 0.00020	0.02303 ± 0.00019
$\Omega_c h^2$	0.1094 ± 0.0010	0.1094 ± 0.0010	0.1094 ± 0.0010
$100\theta_{MC}$	1.04231 ± 0.00041	1.04228 ± 0.00042	1.04229 ± 0.00041
τ	0.119 ± 0.015	0.115 ± 0.011	0.115 ± 0.011
$\ln(10^{10} A_s)$	3.145 ± 0.029	3.138 ± 0.022	3.139 ± 0.022
Ω_k	-0.0075 ± 0.0042	-0.0086 ± 0.0017	-0.0083 ± 0.0016
H_0 [km s $^{-1}$ Mpc $^{-1}$]	68.4 ± 1.9	67.82 ± 0.66	67.93 ± 0.63
Ω_m	0.285 ± 0.016	0.2893 ± 0.0058	0.2885 ± 0.0055
σ_8	0.818 ± 0.014	0.8148 ± 0.0098	0.8156 ± 0.0098
Parameter	TT+lowP+lensing+ $f\sigma_8$	TT+lowP+lensing+NewBAO+ $f\sigma_8$	TT+lowP+lensing+JLA+NewBAO+ $H(z)$ + $f\sigma_8$
$\Omega_b h^2$	0.02305 ± 0.00020	0.02303 ± 0.00020	0.02305 ± 0.00020
$\Omega_c h^2$	0.1090 ± 0.0011	0.1091 ± 0.0011	0.1092 ± 0.0010
$100\theta_{MC}$	1.04229 ± 0.00041	1.04229 ± 0.00041	1.04226 ± 0.00041
τ	0.117 ± 0.019	0.112 ± 0.011	0.113 ± 0.011
$\ln(10^{10} A_s)$	3.141 ± 0.037	3.132 ± 0.022	3.134 ± 0.022
Ω_k	-0.0076 ± 0.0064	-0.0086 ± 0.0017	-0.0082 ± 0.0016
H_0 [km s $^{-1}$ Mpc $^{-1}$]	68.7 ± 3.0	67.93 ± 0.67	68.07 ± 0.63
Ω_m	0.283 ± 0.024	0.2877 ± 0.0058	0.2868 ± 0.0055
σ_8	0.815 ± 0.019	0.8111 ± 0.0098	0.8124 ± 0.0095

duction of the best-fit untilted closed model C_ℓ 's (shown in the lower panels of Figs. 8 and 9) relative to the best-fit tilted flat model C_ℓ 's. Other effects, including the usual and integrated Sachs-Wolfe effects, also play a role in affecting the shape of the low- ℓ C_ℓ 's. For a detailed discussion of how the interplay among these effects influences the low- ℓ shape of the C_ℓ 's in the open inflation case see [Górski et al. \(1998\)](#).

5. CONCLUSION

We use the tilted flat- Λ CDM and the untilted non-flat Λ CDM inflation models to measure cosmological parameters from a carefully gathered compilation of observational data, the largest such collection utilized to date.

Our main results, in summary, are:

- Using a consistent power spectrum for energy density inhomogeneities in the untilted non-flat model, we confirm, with greater significance, the [Ooba et al. \(2018a\)](#) result that cosmological data does not demand spatially-flat hypersurfaces. These data (including CMB lensing measurements) favor a closed Universe at more than 5σ significance, with spatial curvature contributing about a percent to the current cosmological energy budget.

- The best-fit untilted non-flat Λ CDM model provides a better fit to the low- ℓ temperature anisotropy C_ℓ 's and better agrees with the σ_8 - Ω_m DES constraints, but does worse than the best-fit tilted flat- Λ CDM model in fitting the higher- ℓ temperature anisotropy C_ℓ 's.¹⁹
- H_0 measured in both models are almost identical, and consistent with most other measurements of H_0 . However, as is well known, an estimate of the local expansion rate ([Anderson & Riess 2017](#)) is 2.7σ larger.
- σ_8 measured in both models are identical and consistent with the recent DES measurement ([DES Collaboration 2017a](#)).
- The measured Ω_m is more model dependent than the measured σ_8 and the Ω_m value measured using the non-flat Λ CDM model is more consistent with the recent DES measurement ([DES Collaboration 2017a](#)).

¹⁹ We note that the tilted flat XCDM and ϕ CDM models, with dynamical dark energy, provide slightly better fits to the data than does the tilted flat Λ CDM model ([Ooba et al. 2018d](#); [Park & Ratra 2019, 2018a](#); [Solà et al. 2018](#), and references therein).

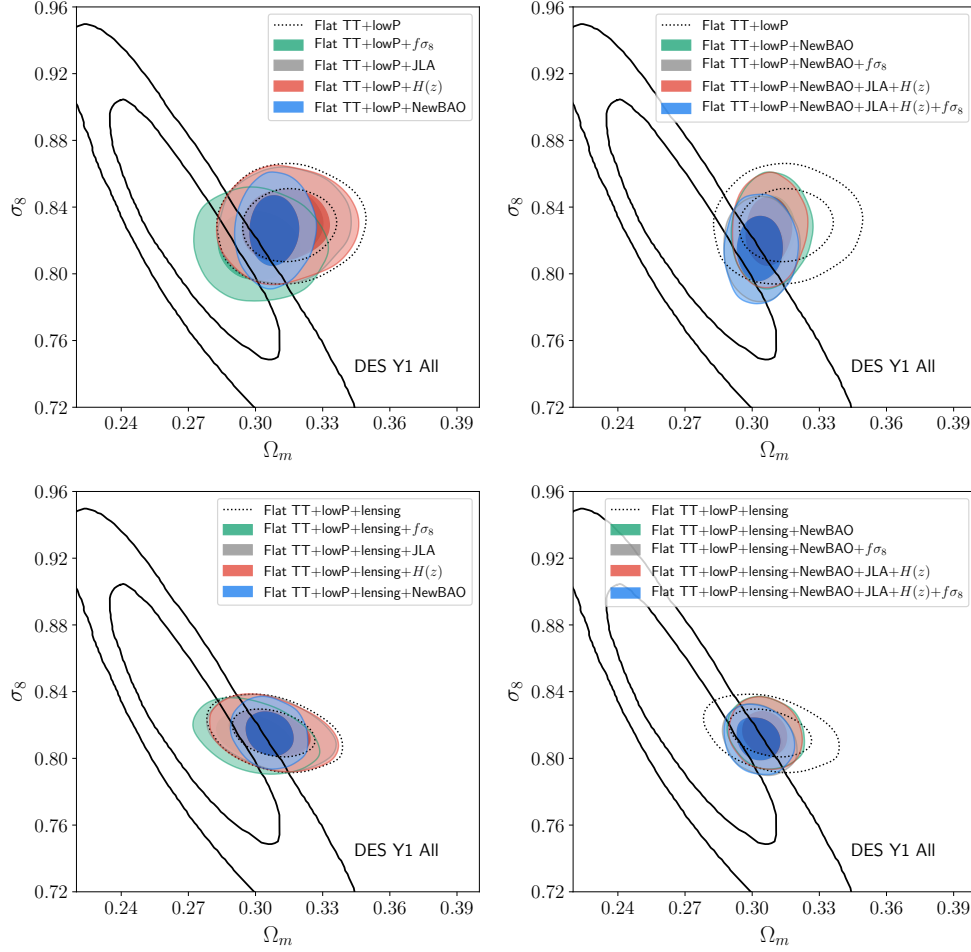


Figure 6. Likelihood distributions in the Ω_m – σ_8 plane for the tilted flat- Λ CDM model constrained by Planck CMB TT + lowP (+lensing), JLA SNIa, NewBAO, $H(z)$, and $f\sigma_8$ data. In each panel the Λ CDM constraints (68.3% and 95.4% confidence limits) obtained from the first-year Dark Energy Survey (DES Y1 All) (DES Collaboration 2017a) are shown as thick solid curves for comparison.

- $\Omega_b h^2$, τ , $\Omega_c h^2$, and some of the other measured cosmological parameter values are quite model dependent. For such parameters, caution is called for when comparing a value measured in a cosmological model to a value determined using another technique.

Overall, the tilted flat- Λ CDM model has a lower χ^2 than the untilted non-flat Λ CDM case and so is more favored. On the other hand, the untilted non-flat Λ CDM model has other advantages, including having a lower σ_8 . It is possible that a more complete understanding of systematic differences between constraints derived using the lower- ℓ and higher- ℓ Planck CMB anisotropy data, as well as a more complete understanding of the differences between the Planck and South Pole Telescope CMB anisotropy data, might have some bearing on these issues.

We acknowledge valuable discussions with J. Ooba. C.-G.P. was supported by the Basic Science Research Program through the National Research Foundation of Korea (NRF) funded by the Ministry of Education (No. 2017R1D1A1B03028384). B.R. was supported in part by DOE grant DE-SC0019038.

REFERENCES

- Addison, G. E., Huang, Y., Watts, D. J., et al. 2016, *ApJ*, 818, 132 [arXiv:1511.00055]
 Alam, S., Ata, M., Bailey, S., et al. 2017, *MNRAS*, 470, 2617 [arXiv:1607.03155]
 Anagnostopoulos, F., & Basilakos, S. 2017, arXiv:1709.02356
 Anderson, L., Aubourg, É., Bailey, S., et al. 2014, *MNRAS*, 441, 24 [arXiv:1312.4877]
 Anderson, R. I., & Riess, A. G. 2017, arXiv:1712.01065
 Ata, M., Baumgarten, F., Bautista, J., et al. 2018, *MNRAS*, 473, 4773 [arXiv:1705.06373]
 Aubourg, É., Bailey, S., Bautista, J. E., et al. 2015, *Phys. Rev. D*, 92, 123516 [arXiv:1411.1074]
 Audren, B., Lesgourgues, J., Benabed, K., & Prunet, S. 2013, *JCAP*, 1302, 001 [arXiv:1210.7183]
 Aylor, K., Hou, Z., Knox, L., et al. 2017, *ApJ*, 850, 101 [arXiv:1706.10286]
 Bautista, J. E., Busca, N. G., Guy, J., et al. 2017, *A&A*, 603, A12 [arXiv:1702.00176]
 Betoule, M., Kessler, R., Guy, J., et al. 2014, *A&A*, 568, A22 [arXiv:1401.4064]
 Beutler, F., Blake, C., Colless, M., et al. 2011, *MNRAS*, 416, 3017 [arXiv:1106.3366]
 Beutler, F., Blake, C., Colless, M., et al. 2012, *MNRAS*, 423, 3430 [arXiv:1204.4725]
 Blake, C., Baldry, I. K., Bland-Hawthorn, J., et al. 2013, *MNRAS*, 436, 3089 [arXiv:1309.5556]
 Blas, D., Lesgourgues, J., & Tram, T. 2011, *JCAP*, 1107, 034 [arXiv:1104.2933]
 Cai, R.-G., Guo, Z.-K., & Yang, T. 2016, *Phys. Rev. D*, 93, 043517 [arXiv:1509.06283]
 Calabrese, E., Archidiacono, M., Melchiorri, A., & Ratra, B. 2012, *Phys. Rev. D*, 86, 043520 [arXiv:1205.6753]
 Cao, S.-L., Duan, X.-W., Meng, X.-L., & Zhang, T.-J. 2018, *Eur. Phys. J.*, C78, 313 [arXiv:1712.01703]
 Challinor, A., & Lasenby, A. 1999, *ApJ*, 513, 1 [arXiv:astro-ph/9804301]

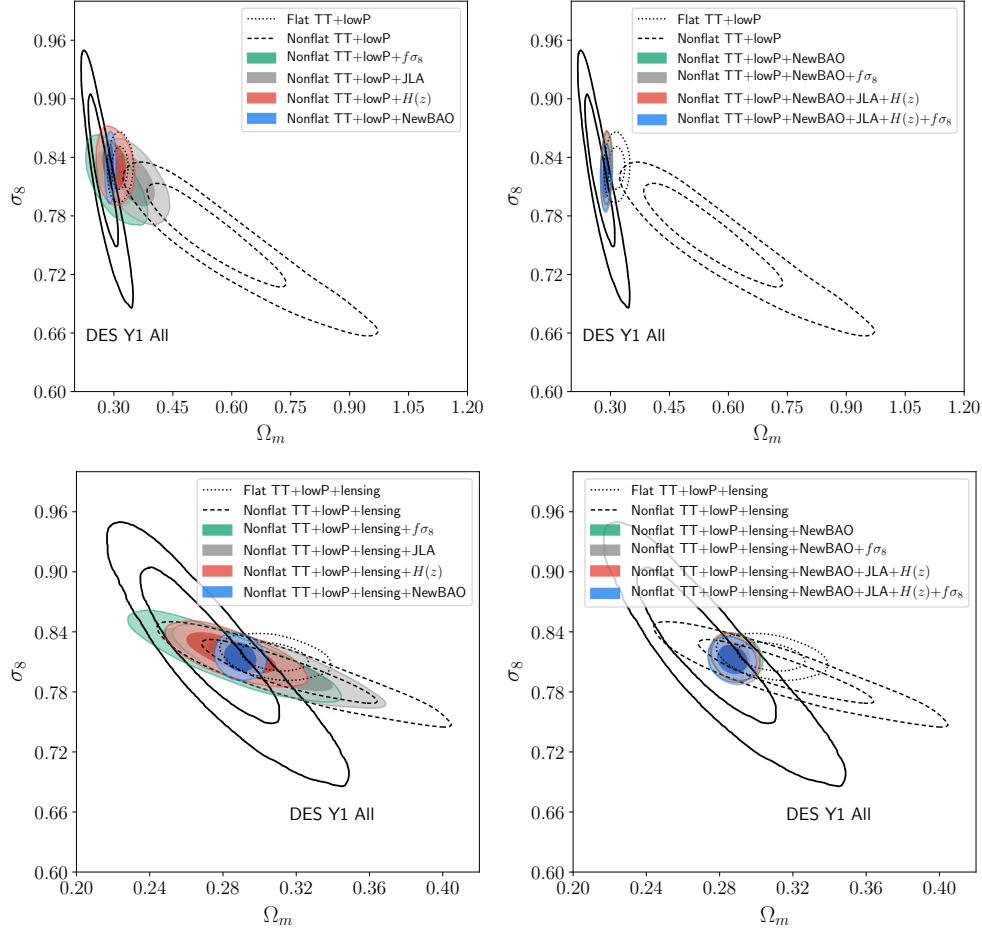


Figure 7. Same as Fig. 6 but for the untitled non-flat Λ CDM model.

Chen, G., Gott, J. R., & Ratra, B. 2003, *PASP*, 115, 1269 [arXiv:astro-ph/0308099]
 Chen, G., & Ratra, B. 2003, *PASP*, 115, 1143 [arXiv:astro-ph/0302002]
 Chen, G., & Ratra, B. 2011a, *PASP*, 123, 1127 [arXiv:1105.5206]
 Chen, Y., Kumar, S., & Ratra, B. 2017, *ApJ*, 835, 86 [arXiv:1606.07316]
 Chen, Y., & Ratra, B. 2011b, *Phys. Lett. B*, 703, 406 [arXiv:1106.4294]
 Chen, Y., Ratra, B., Biesiada, M., Li, S., & Zhu, Z.-H. 2016, *ApJ*, 829, 61 [arXiv:1603.07115]
 Cooke, R. J., Pettini, M., & Steidel, C. C. 2018, *ApJ*, 855, 102 [arXiv:1710.11129]
 DES Collaboration, Abbott, T. M. C., Abdalla, F. B., Alarcon, A., et al. 2017a, arXiv:1708.01530
 DES Collaboration, Abbott, T. M. C., Abdalla, F. B., Annis, J., et al. 2017b, arXiv:1711.00403
 Dhawan, S., Jha, S. W., & Leibundgut, B. 2018, *A&A*, 609, A72 [arXiv:1707.00715]
 Farooq, O., Madiyar, F. R., Crandall, S., & Ratra, B. 2017, *ApJ*, 835, 26 [arXiv:1607.03537]
 Farooq, O., Mania, D., & Ratra, B. 2015, *ApSS*, 357, 11 [arXiv:1308.0834]
 Farooq, O., & Ratra, B. 2013, *ApJ*, 766, L7 [arXiv:1301.5243]
 Feix, M., Nusser, A., & Branchini, E. 2015, *Phys. Rev. Lett.*, 115, 011301 [arXiv:1503.05945]
 Fernández Arenas, D., Terlevich, E., Terlevich, R., et al. 2018, *MNRAS*, 474, 1250 [arXiv:1710.05951]
 Fixsen, D. J. 2009, *ApJ*, 707, 916 [arXiv:0911.1955]
 Font-Ribera, A., Kirkby, D., Busca, N., et al. 2014, *JCAP*, 1405, 027 [arXiv:1311.1767]
 Górski, K. M., Ratra, B., Stompór, R., Sugiyama, N., & Banday, A. J. 1998, *ApJS*, 114, 1 [arXiv:astro-ph/9608054]
 Górski, K. M., Ratra, B., Sugiyama, N., & Banday, A. J. 1995, *ApJ*, 444, L65 [arXiv:astro-ph/9502034]
 Gott, J. R. 1982, *Nature*, 295, 304
 Gott, J. R., Vogeley, M. S., Podariu, S., & Ratra, B. 2001, *ApJ*, 549, 1 [arXiv:astro-ph/0006103]
 Haridasu, B. S., Luković, V. V., & Vittorio, N. 2018, *JCAP*, 1805, 033 [arXiv:1711.03929]
 Hawking, S. W. 1984, *Nucl. Phys. B*, 239, 257

Heavens, A., Fantaye, Y., Mootoooloo, A., et al. 2017, arXiv:1704.03472
 Hinshaw, G., Larson, D., Komatsu, E., et al. 2013, *ApJS*, 208, 19 [arXiv:1212.5226]
 Howlett, C., Ross, A. J., Samushia, L., Percival, W. J., & Manera, M. 2015, *MNRAS*, 449, 848 [arXiv:1409.3238]
 Hudson, M. J., & Turnbull, S. J. 2012, *ApJ*, 751, L30 [arXiv:1203.4814]
 Huterer, D., & Shafer, D. L. 2017, arXiv:1709.01091
 Kamionkowski, M., Ratra, B., Spergel, D. N., & Sugiyama, N. 1994, *ApJ*, 434, L1 [arXiv:astro-ph/9406069]
 Lewis, A., & Bridle, S. 2002, *Phys. Rev. D*, 66, 103511 [arXiv:astro-ph/0205436]
 Lewis, A., Challinor, A., & Lasenby, A. 2000, *ApJ*, 538, 473 [arXiv:astro-ph/9911177]
 L'Huillier, B., & Shafieloo, A. 2017, *JCAP*, 1701, 015 [arXiv:1606.06832]
 Li, Z., Wang, G.-J., Liao, K., & Zhu, Z.-H. 2016, *ApJ*, 833, 240 [arXiv:1611.00359]
 Lin, W., & Ishak, M. 2017, *Phys. Rev. D*, 96, 083532 [arXiv:1708.09813]
 Lonappan, A. I., Ruchika, & Sen, A. A. 2017, arXiv:1705.07336
 Lucchin, F., & Matarrese, S. 1985, *Phys. Rev. D*, 32, 1316
 Luković, V. V., D'Agostino, R., & Vittorio, N. 2016, *A&A*, 595, A109 [arXiv:1607.05677]
 Magana, J., Amante, M. H., Garcia-Aspeitia, M. A., & Motta, V. 2017, arXiv:1706.09848
 Martin, J. 2012, *C. R. Physique*, 13, 566 [arXiv:1205.3365]
 Mitra, S., Choudhury, T. R., & Ratra, B. 2018, *MNRAS*, 479, 4566 [arXiv:1712.00018]
 Mitra, S., Park, C.-G., Choudhury, T. R., & Ratra, B. 2019, arXiv:1901.09927
 Moresco, M. 2015, *MNRAS*, 450, L16 [arXiv:1503.01116]
 Moresco, M., Cimatti, A., Jimenez, R., et al. 2012, *JCAP*, 1208, 006 [arXiv:1201.3609]
 Moresco, M., Pozzetti, L., Cimatti, A., et al. 2016, *JCAP*, 1605, 014 [arXiv:1601.01701]
 Okumura, T., Hikage, C., Totani, T., et al. 2016, *PASJ*, 68, 38 [arXiv:1511.08083]
 Ooba, J., Ratra, B., & Sugiyama, N. 2018a, *ApJ*, 864, 80 [arXiv:1707.03452]

Table 9
Individual and total χ^2 values for the best-fit tilted flat and untilted non-flat Λ CDM inflation models.

Data sets	χ^2_{Plik}	χ^2_{lowTEB}	χ^2_{lensing}	χ^2_{JLA}	χ^2_{NewBAO}	$\chi^2_{H(z)}$	$\chi^2_{f\sigma_8}$	χ^2_{prior}	Total χ^2	$\Delta\chi^2$	$\ln B$
Tilted flat- Λ CDM model											
TT+lowP	763.57	10496.41						1.96	11261.93		
+JLA	763.60	10496.48		695.32				1.92	11957.32		
+NewBAO	762.50	10497.73			13.46			2.36	11276.05		
+ $H(z)$	763.98	10496.36				14.89		1.70	11276.93		
+ $f\sigma_8$	766.83	10494.95					12.15	1.87	11275.80		
+NewBAO+ $f\sigma_8$	766.47	10494.93			12.63		12.45	2.02	11288.50		
+JLA+NewBAO	764.11	10496.10		695.17	12.91			2.21	11970.51		
+JLA+NewBAO+ $H(z)$	764.30	10496.06		695.19	12.94	14.81		1.95	11985.25		
+JLA+NewBAO+ $H(z)$ + $f\sigma_8$	766.81	10494.80		695.12	12.73	14.79	12.15	2.05	11998.43		
TT+lowP+lensing	766.20	10494.93	9.30					2.00	11272.44		
+JLA	767.15	10494.77	8.98	695.07				2.18	11968.15		
+NewBAO	766.37	10494.86	9.12		12.59			2.11	11285.06		
+ $H(z)$	766.20	10494.92	9.27			14.83		2.04	11287.27		
+ $f\sigma_8$	768.26	10494.43	8.67				11.31	1.94	11284.62		
+NewBAO+ $f\sigma_8$	767.47	10494.57	8.73		12.66		11.80	2.11	11297.33		
+JLA+NewBAO	766.42	10494.85	9.16	695.19	12.61			2.01	11980.24		
+JLA+NewBAO+ $H(z)$	766.57	10494.76	9.04	695.16	12.59	14.81		2.15	11995.08		
+JLA+NewBAO+ $H(z)$ + $f\sigma_8$	767.50	10494.56	8.74	695.12	12.65	14.79	11.79	2.07	12007.21		
Untilted non-flat Λ CDM model											
TT+lowP	774.34	10495.42						2.33	11272.10	10.17	-5.63
+JLA	771.82	10503.02		696.54				2.40	11973.80	16.48	-7.09
+NewBAO	779.37	10499.98			14.25			1.95	11295.55	19.50	-11.2
+ $H(z)$	777.14	10500.93				17.11		1.96	11297.15	20.22	-11.1
+ $f\sigma_8$	783.38	10497.49					11.51	2.41	11294.79	18.99	-9.72
+NewBAO+ $f\sigma_8$	781.01	10500.07			14.32		11.25	1.97	11308.62	20.12	-10.1
+JLA+NewBAO	784.80	10496.68		695.18	13.95			2.29	11992.90	22.39	-9.42
+JLA+NewBAO+ $H(z)$	779.51	10500.26		695.17	14.18	16.08		1.98	12007.20	21.95	-11.9
+JLA+NewBAO+ $H(z)$ + $f\sigma_8$	784.11	10497.49		695.20	13.95	16.36	10.61	1.82	12019.53	21.10	-10.8
TT+lowP+lensing	786.87	10493.86	9.77					1.79	11292.29	19.85	-10.5
+JLA	786.10	10494.47	9.87	695.22				2.07	11987.73	19.58	-8.99
+NewBAO	784.85	10496.56	9.42		13.81			1.87	11306.51	21.45	-9.89
+ $H(z)$	786.87	10496.02	8.66			16.36		2.19	11310.10	22.83	-11.4
+ $f\sigma_8$	786.41	10496.00	8.75				9.79	1.99	11302.93	18.31	-9.60
+NewBAO+ $f\sigma_8$	786.11	10495.99	8.86		13.80		9.96	1.84	11316.56	19.23	-10.3
+JLA+NewBAO	786.53	10495.26	8.83	695.17	13.67			1.93	12001.40	21.16	-11.3
+JLA+NewBAO+ $H(z)$	787.20	10495.41	8.56	695.19	13.78	16.36		1.85	12018.35	23.27	-12.0
+JLA+NewBAO+ $H(z)$ + $f\sigma_8$	786.97	10495.48	8.71	695.20	13.74	16.29	9.87	1.92	12028.17	20.96	-11.0

Note: $\Delta\chi^2$ and $\ln B$ of a non-flat Λ CDM model estimated for a combination of data sets represent the excess χ^2 value and ratio of Bayesian evidence, respectively, relative to the tilted flat model for the same combination of data sets.

Ooba, J., Ratra, B., & Sugiyama, N. 2018b, *ApJ*, 869, 34 [arXiv:1710.03271]
Ooba, J., Ratra, B., & Sugiyama, N. 2018c, *ApJ*, 866, 68 [arXiv:1712.08617]
Ooba, J., Ratra, B., & Sugiyama, N. 2018d, arXiv:1802.05571
Park, C.-G., & Ratra, B. 2019, *ApSS*, in press [arXiv:1803.05522]
Park, C.-G., & Ratra, B. 2018a, *ApJ*, 868, 83 [arXiv:1807.07421]
Park, C.-G., & Ratra, B. 2018b, arXiv:1809.03598
Pavlov, A., Westmoreland, S., Saaidi, K., & Ratra, B. 2013, *Phys. Rev. D*, 88, 123513 [arXiv:1307.7399]
Peebles, P. J. E. 1984, *ApJ*, 284, 439
Peebles, P. J. E., & Ratra, B. 1988, *ApJ*, 325, L17
Penton, J., Peyton, J., Zahoor, A., & Ratra, B. 2018, *PASP*, 130, 114009 [arXiv:1808.01490]
Pezzotta, A., de la Torre, S., Bel, J., et al. 2017, *A&A*, 604, A33 [arXiv:1612.05645]
Planck Collaboration, Ade, P. A. R., Aghanim, N., Armitage-Caplan, C., et al. 2014, *A&A*, 571, A16 [arXiv:1303.5076]
Planck Collaboration 2015, *Planck* 2015 Results: Cosmological Parameter Tables at wiki.cosmos.esa.int/planckpla2015/images/t/f7/Baseline_parameters_table_2015_limit68.pdf

Planck Collaboration, Ade, P. A. R., Aghanim, N., Arnaud, M., et al. 2016, *A&A*, 594, A13 [arXiv:1502.01589]
Planck Collaboration, Aghanim, N., Akrami, Y., Ashdown, M., et al. 20167, *A&A*, 607, A95 [arXiv:1608.02487]
Podariu, S., & Ratra, B. 2001, *ApJ*, 532, 109 [arXiv:astro-ph/9910527]
Rana, A., Jain, D., Mahajan, S., & Mukherjee, A. 2017, *JCAP*, 1703, 028 [arXiv:1611.07196]
Ratra, B. 1985, *Phys. Rev. D*, 31, 1931
Ratra, B. 1989, *Phys. Rev. D*, 40, 3939
Ratra, B. 1992, *Phys. Rev. D*, 45, 1913
Ratra, B. 2017, *Phys. Rev. D*, 96, 103534 [arXiv:1707.03439]
Ratra, B., & Peebles, P. J. E. 1988, *Phys. Rev. D*, 37, 3406
Ratra, B., & Peebles, P. J. E. 1994, *ApJ*, 432, L5
Ratra, B., & Peebles, P. J. E. 1995, *Phys. Rev. D*, 52, 1837
Ratra, B., & Vogeley, M. 2008, *PASP*, 120, 235 [arXiv:0706.1565]
Ratsimbazafy, A. L., Loubser, S. I., Crawford, S. M., et al. 2017, *MNRAS*, 467, 3239 [arXiv:1702.00418]
Rezaei, M., Malekjani, M., Basilakos, S., Mehrabi, A., & Mota, D. F. 2017, *ApJ*, 843, 65 [arXiv:1706.02537]

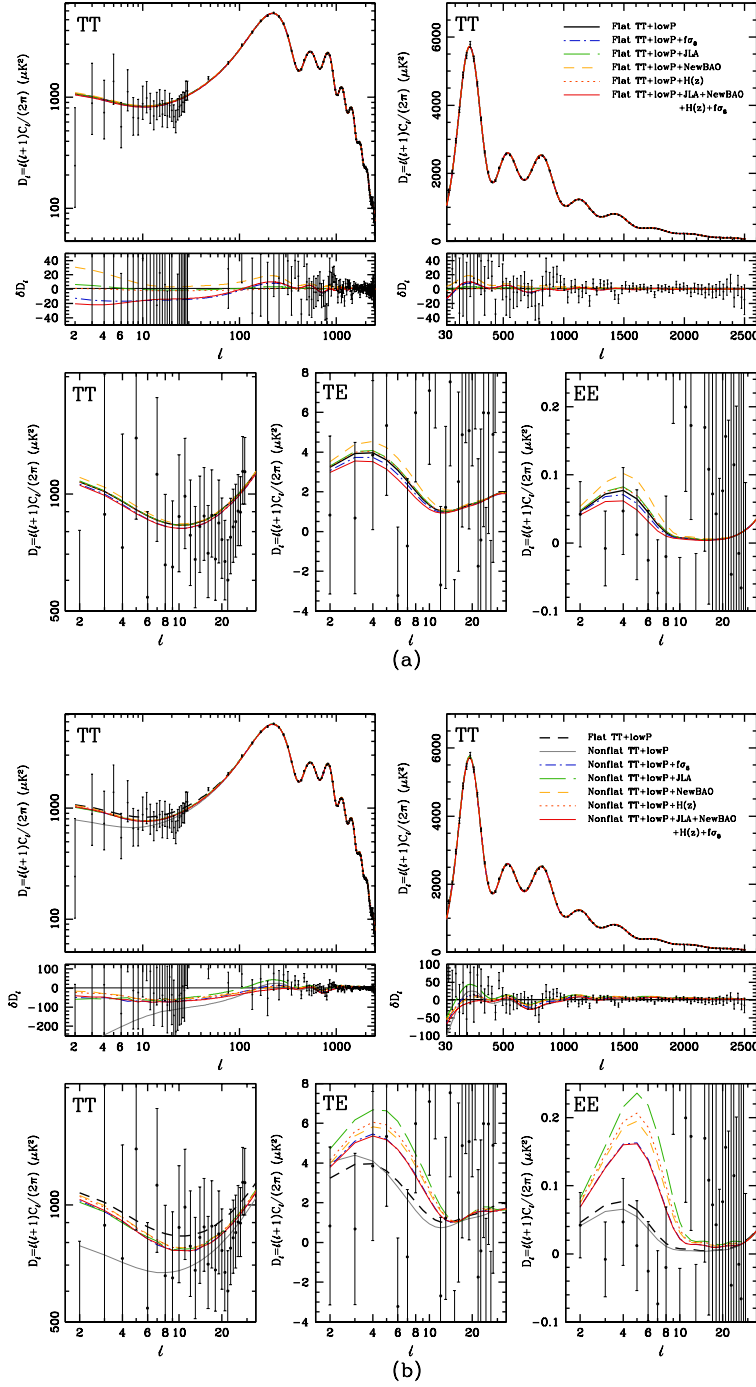


Figure 8. Best-fit power spectra of (a) tilted flat (top five panels) and (b) untitled non-flat Λ CDM models (bottom five panels) constrained by the Planck CMB TT + lowP data (excluding the lensing data) together with JLA SNIa, NewBAO, $H(z)$, and $f\sigma_8$ data.

Rigault, M., Aldering, G., Kowalski, M., et al. 2015, *ApJ*, 802, 20 [arXiv:1412.6501]
 Ross, A. J., Samushia, L., Howlett, C., et al. 2015, *MNRAS*, 449, 835 [arXiv:1409.3242]
 Ryan, J., Chen, Y., & Ratra, B. 2019, arXiv:1902.03196
 Ryan, J., Doshi, S., & Ratra, B. 2018, *MNRAS*, 480, 759 [arXiv:1805.06408]
 Samushia, L., Chen, G., & Ratra, B. 2007, arXiv:0706.1963
 Samushia, L., & Ratra, B. 2006, *ApJ*, 650, L5 [arXiv:astro-ph/0607301]
 Sievers, J. L., Hlozek, R. A., Nolte, M. R., et al. 2013, *JCAP*, 1310, 060 [arXiv:1301.0824]

Simon, J., Verde, L., & Jimenez, R. 2005, *Phys. Rev. D*, 71, 123001 [arXiv:astro-ph/0412269]
 Simpson, F., Blake, C., Peacock, J. A., et al. 2016, *Phys. Rev. D*, 93, 023525 [arXiv:1505.03865]
 Solà, J., Gómez-Valent, A., & de Cruz Pérez, J. 2018, arXiv:1811.03505
 Springob, C. M., Hong, T., Staveley-Smith, L., et al. 2016, *MNRAS*, 456, 1886 [arXiv:1511.04849]
 Stern, D., Jimenez, R., Verde, L., Kamionkowski, M., & Stanford, S. A. 2010, *JCAP*, 1002, 008 [arXiv:0907.3152]
 Tripathi, A., Sangwan, A., & Jassal, H. K. 2017, *JCAP*, 1706, 012 [arXiv:1611.01899]
 Trotta, R. 2008, *Contemp. Phys.* 49, 71 [arXiv:0803.4089]

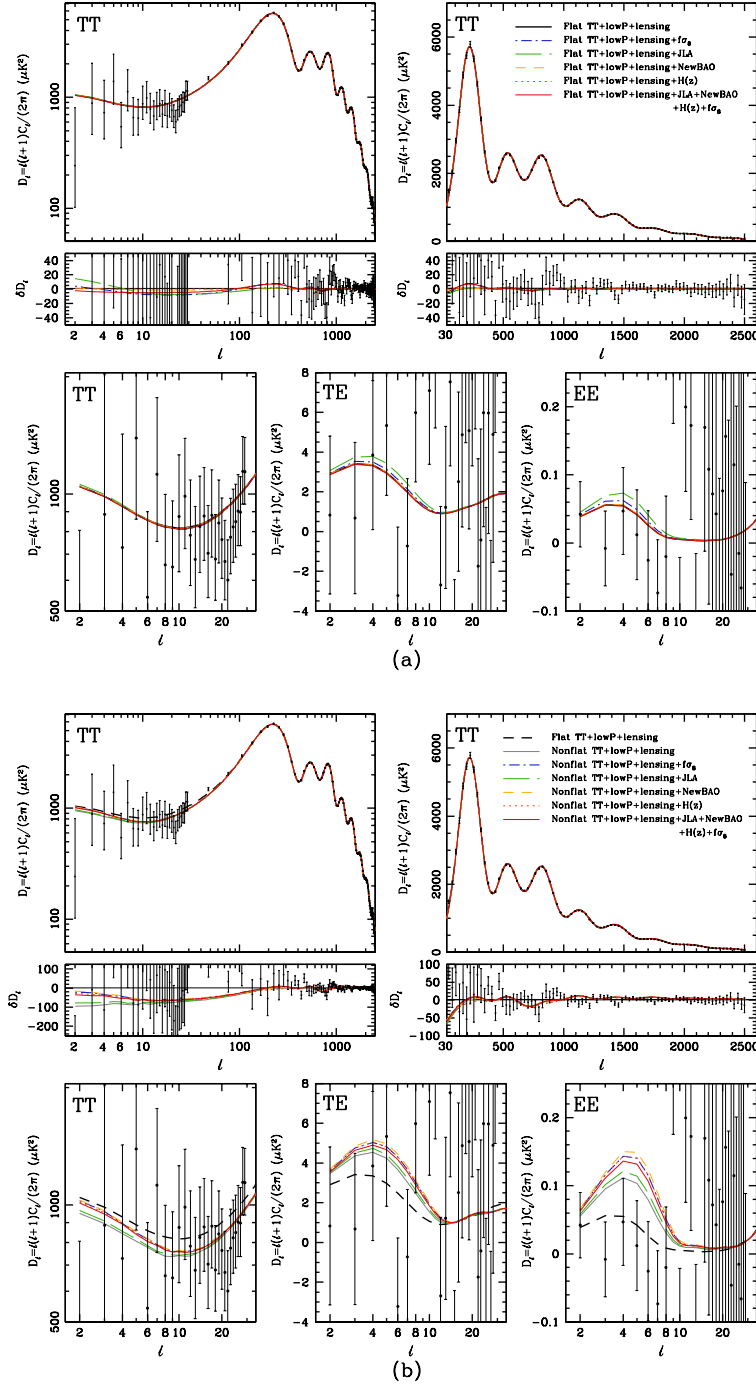


Figure 9. Same as Fig. 8 but now including the lensing data.

Turnbull, S. J., Hudson, M. J., Feldman, H. A., et al. 2012, MNRAS, 420, 447 [arXiv:1111.0631]
Wang, Y., Xu, L., & Zhao, G.-B. 2017, arXiv:1706.09149
Wei, J.-J., & Wu, X.-F. 2017, ApJ, 838, 160 [arXiv:1611.00904]
Yu, H., Ratra, B., & Wang, F.-Y. 2018, ApJ, 856, 3 [arXiv:1711.03437]
Yu, H., & Wang, F. Y. 2016, ApJ, 828, 85 [arXiv:1605.02483]

Zhang, B. R., Childress, M. J., Davis, T. M., et al. 2017, MNRAS, 471, 2254 [arXiv:1706.07573]
Zhang, C., Zhang, H., Yuan, S., Zhang, T.-J., & Sun, Y.-C. 2014, Res. Astron. Astrophys., 14, 1221 [arXiv:1207.4541]

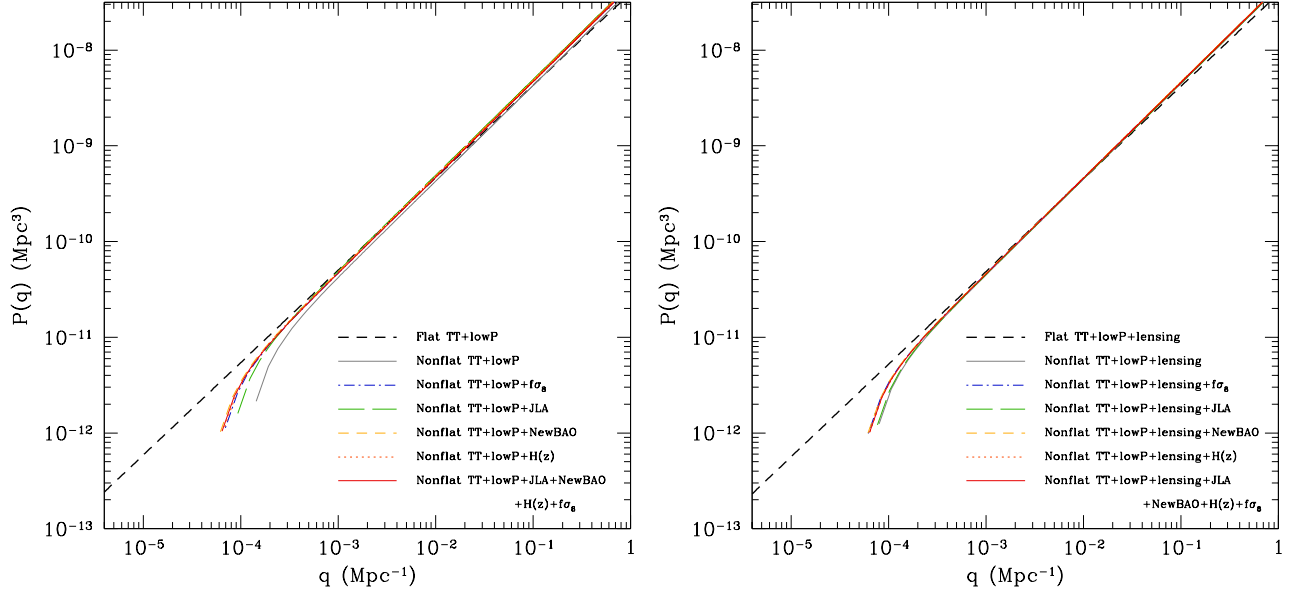


Figure 10. Power spectra of primordial scalar-type perturbations constrained by Planck TT + lowP data (left panel) and TT + lowP + lensing data (right panel). In both panels the primordial power spectrum of the best-fit tilted flat- Λ CDM model is shown as dashed curves. Note that the power spectrum of each untitled non-flat model has discrete points of normal modes with positive integers $\nu = qK^{-1/2} = 3, 4, 5, \dots$, where $q = \sqrt{k^2 + K}$ and K is the spatial curvature. The power spectrum is normalized to $P(q) = A_s$ at the pivot scale $k_0 = 0.05 \text{ Mpc}^{-1}$.